Catastrophic Collapse Features in Volcanic Terrains: Styles and Links to Subvolcanic Magma Systems

David B. Hacker, Peter D. Rowley and Robert F. Biek

Abstract

Catastrophic structural slope failures of large volcanic landforms, notably volcanoes, are among the most sudden agents of landscape change, producing large-scale landslide features. Some of these volcanic landslides rank among the largest and most devastating natural hazards encountered on Earth. Following the 1980 landslide and directed blast that destroyed the northern flank of Mount St. Helens, there has been an increased awareness and study of flank and sector collapses of stratovolcanoes worldwide. Collapse features have now been observed on hundreds of volcanoes and it is now widely accepted that such events are common recurrent phenomena during the evolution of many volcanoes. Although most studies of structural failure have concentrated on volcanoes, it is important to note that two other volcanic landforms in volcanic terrains have experienced collapse events at scales equivalent to, and sometimes exceeding, the scale of landslides on volcanoes. These include slope failures from intrusive laccoliths and from partial collapse of volcanic fields. Volcanic landslides from these less familiar sources share many morphological and textural similarities as landslides from volcanoes and could be mistaken as a volcano-derived deposit. Subvolcanic magma systems play an integral part in the collapse process from these three volcanic source types (volcanoes, laccoliths, and volcanic fields) by creating elevated landforms with steep slopes, aiding in destabilization of

D.B. Hacker (✉)
Department of Geology, Kent State University, Kent, OH, USA
e-mail: dhacker@kent.edu

P.D. Rowley
Geologic Mapping Inc., New Harmony, UT, USA

R.F. Biek
Utah Geological Survey, Salt Lake City, UT, USA

Advs in Volcanology (2018) 215–248
DOI 10.1007/11157_2017_1001

Published Online: 10 April 2017

the slopes, and often triggering a slope failure. We therefore introduce a new concept that volcanic collapse landslide features should be viewed as involving multiple sources within volcanic terrains instead of from only volcanoes.

1 Introduction

Volcanic terrains are the surface expressions of magma reaching the surface of our planet from the interior, often through a complex subsurface plumbing system. These dynamic terrains consist of a great variety of volcanic rock types, from lavas and explosive pyroclastics to secondary epiclastic deposits. They also contain a wide variety of volcanic landforms, consisting largely of volcanoes of diverse shapes and forms, including calderas, lava domes, outflow tuff plains, and lava plateaus. Also present is a pervasive array of shallow subvolcanic intrusions of dikes, sills, and laccoliths, many of which were themselves conduits for explosive or effusive volcanic eruptions. Prior to significant buildout of volcanic landforms, early ash deposited in lake, stream, and marine environments may in time break down into soft expansive clays and therefore result in a weak foundation for the later rapid and voluminous accumulation of heavy volcanic deposits on this foundation. During the evolution of a volcanic field, its growth (constructive buildup phases) of surface volcanic features is constantly under attack by gravity and erosion that acts to reduce them (destructive phases). As part of this interplay of volcanic growth and erosion, elevated volcanoes have frequently been punctuated by catastrophic gravitational collapse of their edifices, producing volcanic landslides that moved large rock masses kilometers to hundreds of kilometers from their source.

Interest in volcanic landslides took off over the past few decades following the spectacular 1980 sector collapse and eruption of Mount St. Helens volcano (Fig. 1). Subsequent studies have recognized collapse events on more than 400 volcanoes worldwide (Siebert et al. 2006). Terrestrial volcano collapses can produce large volumes (greater than several km^3) of rock material that move downslope at high velocities (greater than 100 m/s) and travel distances sometimes exceeding 50 km, forming deposits spread over areas of hundreds to thousands of km^2 (Ui 1983; Siebert 1984, 1992, 1996, 2002; Schuster and Crandell 1984; Ui et al. 2000; van Wyk de Vries and Davies 2015). Large sector collapses have occurred at a rate of approximately 4–5 per century over the last 500 years, a rate roughly double that of caldera collapse following magma chamber evacuation during the same interval (Siebert et al. 2010). Discovery of submarine volcanic and non-volcanic landslides has shown that they are even larger, with volumes of as much as 5000 km^3, travel distances exceeding 200 km, and have depositional areas of as much as 23,000 km^2 (Moore et al. 1989, 1994; Carracedo 1994). Similarly, volcano collapses are not confined to Earth, but have also been discovered on both Mars (Crumpler et al. 1996) and Venus (Bulmer and Guest 1996).

However, we are now becoming aware that not all volcanic landslides necessarily originate only from collapse of volcanoes. Intrusive laccoliths, and even large portions of volcanic fields have experienced structural failure in the past leading to catastrophic volcanic landslides and initiation of volcanic eruptions (Hacker 1998; Hacker et al. 2007; Rowley et al. 2006; Biek et al. 2009, 2015). Batholiths beneath volcanic fields can produce the rapid and considerable relief necessary for slope failure, whether by feeding shallow, higher level laccoliths, or by uplifting and tilting (magma inflation) a large portion of a volcanic field itself. We emphasize here that recognition of ancient landslides in a

Fig. 1 North Fork Toutle River valley, Mount St. Helens, Washington. A scientist stands on one of the many hummocks that form the chaotic surface of a massive volcanic landslide deposit in the upper North Fork Toutle River valley below Mount St. Helens volcano (10 km in distance). Before the landslide and eruption on May 18, 1980, a forest grew on this part of the valley floor. The landslide deposit extends about 22 km from the volcano and buries the river valley to an average depth of about 45 m. In places, the deposit is nearly 200 m thick. The landslide covers an area of about 60 km^2. Photograph by L. Topinka in 1981, courtesy of the USGS

volcanic terrain need not automatically be attributed to collapse of an individual volcano, especially in the absence of a documented edifice, but could also have originated from alternative volcanic causes whose modern hazard assessment is still in its infancy.

The growing need for better understanding of landslide processes operating in volcanic terrains stems from the societal need of protecting human populations from these rare but high impact hazards. Volcanic landslide generation poses a considerable hazard for inhabited areas around volcanoes, either directly or through secondary events, such as tsunamis (Keating and McGuire 2000), lahars (Scott et al. 2005), or magmatic eruptions (Lipman et al. 1991). They have caused approximately 20,000 casualties in the last 400 years (Siebert 1984) and millions of people currently live on top of volcanic landslide deposits (Siebert 2002), where recurrent collapses are possible (e.g., Komorowski et al. 2005). Studies in both modern and ancient volcanic terrains have contributed to the major growth of understanding the physical processes involved in volcanic landslides. Although the studies of volcano collapse hazards are highly warranted, awareness of collapse from other volcanic sources should be kept in mind when documenting and assessing the geologic structure and evolution of modern volcanic fields. Although large-scale catastrophic collapse of volcanic fields are rare, they represent the largest known subaerial volcanic landslides on Earth (Hacker et al. 2014).

In this short overview, we introduce the concept of volcanic landslides originating from multiple volcanic landform sources within volcanic terrains. Collapses due to volcano buildup, laccolith emplacement, and deposition of large parts of volcanic fields themselves will be

emphasized. Although volcanic landslides from laccoliths and volcanic fields are less well known, they have produced similar volcanic landslide deposits as those from volcanoes, but often on a much larger scale. We will concentrate on the subaerial volcanic landslides and collapse events generated from three volcanic landform types (i.e., volcanoes, laccoliths, and volcanic fields) and review the common causes and triggers of collapse related to magmatic activity within the subvolcanic plumbing system. A review of collapse features and submarine volcanic landslides from marine volcanoes can be found in McGuire (2006).

2 Volcanic Landslides

Catastrophic structural failure (collapse) from volcanoes, laccoliths, and volcanic fields generate many types of similar landslides. Engineering geologists include as landslides all types of mass movements, including falls, topples, slides (including slumps), spreads, and flows (Varnes 1978; Cruden and Varnes 1996). In volcanic terrains, the full spectrum of these "landslide" movements occur, but the most common catastrophic collapse mass movements involve slides and flows. Major volcanic, as well as nonvolcanic, mass movements are typically complex, involving various combinations of slide and flow processes within different parts of the moving mass during different stages of development (Varnes 1978; Voight 1978). Volcanic landslides have been variably called a flank failure, flank collapse, sector collapse, rockslide, debris avalanche, rockslide-debris avalanche, rockslide-avalanche, and gravity slide (e.g., Crandell et al. 1984; Siebert 1984, 2002; Glicken 1996; van Wyk de Vries and Francis 1997; Hacker 1998). The term "volcanic landslide" used here describes a variety of slide and flow processes and mass movements involving gravity-driven, downward and outward transfer of wet or dry slope-forming materials (rock, debris, soil, etc.) from its collapsed source to an area of deposition. Therefore we include three depositional types, namely slide, debris avalanche, and debris flow in the term volcanic landslide (Fig. 2).

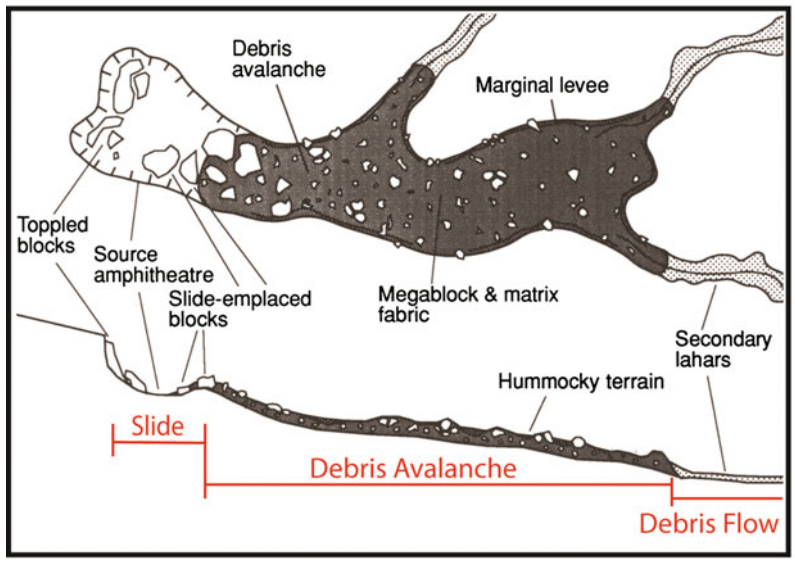

Fig. 2 Anatomy of a volcanic landslide illustrating the slide-debris avalanche-debris flow transitions (*above* map view; *below* schematic section). Characteristic features include a slide zone of relatively coherent blocks (or toreva blocks) emplaced by sliding or toppling in the source area; a debris avalanche zone containing megablocks and matrix facies forming a hummocky terrain bounded by marginal levees; a debris flow zone (or secondary lahars) flowing in channels. Modified from McGuire (1996)

Volcanic mass movements commonly begin with a sliding mass, although flow soon dominates in the form of debris avalanches and/or debris flows as movement progresses (Fig. 2). Large segments of volcanic material can slide downslope without transforming into debris avalanches. In most cases, disaggregation rapidly transforms movement into fragmental flow of debris avalanches that rapidly attain high velocities over low-angle terrains. Therefore, volcanic landslides can be viewed as a continuous sequence of emplacement events with the resulting deposit being dominated by one type, or in some cases, a combination of all three (i.e., slide, debris avalanche, and debris flow). Most often, the lines of separation are blurred and there is a gradation between them. However, these three types display distinct structural patterns and kinetic behavior and will be discussed separately below.

2.1 Volcanic Slides

The volcanic landslide sequence outlined above begins with sliding of a large mass of rock from a source area. In volcanic slides, the displaced rock mass moves as an essentially coherent unit or units of broken blocks under the influence of gravity while maintaining contact with the substrate as it shears over it (Fig. 2). Barely perceptible movements of a rock mass can pass through a stage of accelerating creep into a rapid downward and outward displacement of a rock slide mass along one or several surfaces. Initial movements can be divided into translational (block slide) or rotational (slump) types that involve lateral movement of the slide mass or individual discrete slide blocks bounded by normal (extensional) faults. Slides in volcanic terrains should be very common due to steep slopes and the interbedding of mechanically diverse lithologies such as pyroclastic, epiclastic, and lava flow units. Being relatively coherent, slides retain elements of original stratigraphy with some degree of internal deformation such as minor faults and folds. The source area will often be marked by a scar that is commonly concave in the direction of movement. Stranded detached slabs, or blocks, may mark a trail of the slide mass back to the scar (see Fig. 2). Nonvolcanic slides share similarities with volcanic slides and have been well documented in the subaerial and subaqueous environments (e.g. Voight 1978).

Large backward tilted and rotated blocks on the scale of several kilometers have been termed "toreva blocks" and can travel several kilometers in a nearly coherent manner. At Socampa volcano in Chile, toreva blocks traveled 7 km from their source without disaggregating into an avalanche deposit (Francis et al. 1985; Wadge et al. 1995) and 9 km at Barú volcano in Panama (Herrick et al. 2013).

2.2 Volcanic Debris Avalanches

A debris avalanche is a common middle stage in the transformation sequence from slide to debris flow (Fig. 2). A volcanic debris avalanche is referred to as a rapidly moving heterogeneous, unsorted mass of rock and soil mobilized by gravity from its source (Schuster and Crandell 1984). Volcanic debris avalanches form when frontal sections of the slide mass disintegrates upon continued movement through shear under gravity. As the slide mass section leaves the source area it collapses into a granular flow and travels over the landscape at high velocities (as much as $\sim$100 m/s) spreading and thinning as it moves (Davies et al. 2010). After traveling many kilometers, the mass decelerates to rest, leaving a deposit (may be over 100 km long) containing all or some of the following features: (1) highly comminuted debris, (2) prominent hummocky terrain consisting of conical to elongated mounds on the surface, (3) raised marginal edges forming levees (see Fig. 2; McGuire 1996; Davies et al. 2010). Hummocks are often an indicator of extensional spreading (e.g., Voight 1981; Glicken 1998; Ponomareva et al. 2006; Shea et al. Shea et al. 2008). Detailed deposit descriptions exist for debris avalanche events such as Mount St. Helens (Glicken 1998), Socompa (van Wyk de Vries et al. 2001), Mombacho (Shea et al. 2008), and Parinacota (Clavero et al. 2002).

In general the moving rock mass flows, rather than slides, and the shearing action with the substrate is low (Hsü 1975, 1978; Ui 1983; Siebert 1984). Pervasive internal deformation occurs during movement, and the resultant clasts have a degree of relative motion and freedom between each other. The inertial Bagnoldian grain flow mechanics of avalanches means that grain support, grain momentum, and flow momentum are all maintained by grain-to-grain collisions leading to a progressive transfer of momentum through the flow (Hsü 1978; Pierson and Costa 1987; Iverson 1997). Avalanches are therefore incoherent and have considerable interactions between clasts, making the flow highly mobile. Deposition takes place through frictional freezing of the rock mass as it loses momentum, showing that the avalanche flow has a relatively high bulk viscosity and a high degree of clast interaction.

2.3 Volcanic Debris Flows

Debris flows are commonly the final stage of transformation within the volcanic landslide sequence (Fig. 2). A debris flow is typically a flowing mixture of debris and water, with sediment concentrations between 70 and 90% by weight (Pierson and Costa 1987). Volcanic debris flows are commonly referred to as lahars and can transform to even more dilute flows called hyperconcentrated flows with the addition of more water. If the landside is large enough and contains a high-enough percentage of water and fine material (typically, >3–5% of clay-sized particles), these secondary flows can reach longer distances than the debris avalanches, sometimes traveling as much as 200 km downstream.

Volcanic debris flows owe much of their behavior to excess pore-water pressure and a pore fluid that is viscous and contains fine sediment. In cases of very hot lahars, steam may contribute to mobility (Arguden and Rodolfo 1990). A moving lahar looks like a roiling rapid slurry of wet concrete. As it travels downstream, the size, speed, and amount of material carried can constantly change. The initial flow may be relatively small, but a debris flow may grow in volume as it entrains (called bulking) and incorporates anything in its path, including rocks, soil, vegetation; and even buildings, cars, and bridges. The flowing slurry may consume additional water through melting of snow and ice or by engulfing river or lake water and can grow to more than 10 times its initial size as it moves downslope. In steep areas lahar speeds can exceed 55 m/s.

Debris flows associated with volcanic landslides originate from: (1) direct transformation of a debris avalanche during its long transport (Scott et al. 2002); (2) transformation of the distal portion of a more water-saturated debris avalanche (Palmer and Neall 1989); (3) post-depositional remobilization of water-saturated parts of a debris avalanche (Glicken 1998; Pulgarin et al. 1999); and (4) subsequent rupture of natural dams formed by the earlier obstruction of drainages during the emplacement of a debris-avalanche deposit (Costa 1988; Costa and Shuster 1988). The first two types take place during the related collapse event or maybe some hours later. In contrast, the last two types can occur following an indeterminate lapse of time ranging from hours to years (Costa and Shuster 1988).

2.4 Mount St. Helens, USA: Classic Case Study of Cataclysmic Collapse and Eruption

The largest and best known historically witnessed volcanic landslide in a volcanic terrain was the catastrophic event that initiated the devastating 1980 eruption of Mount St. Helens (Cascade Range, USA). On May 18, 1980, the northern sector of Mount St. Helens failed retrogressively and led to the formation of a 2.5 km^3 volcanic landslide (Lipman and Mullineaux 1981; Voight 1981; Glicken 1998). Magma began intruding into the Mount St. Helens edifice in early spring of 1980 and by May 18, a cryptodome (forming the "bulge") on the northern flank (Fig. 3a) had deformed the edifice to the point of instability. By that time,

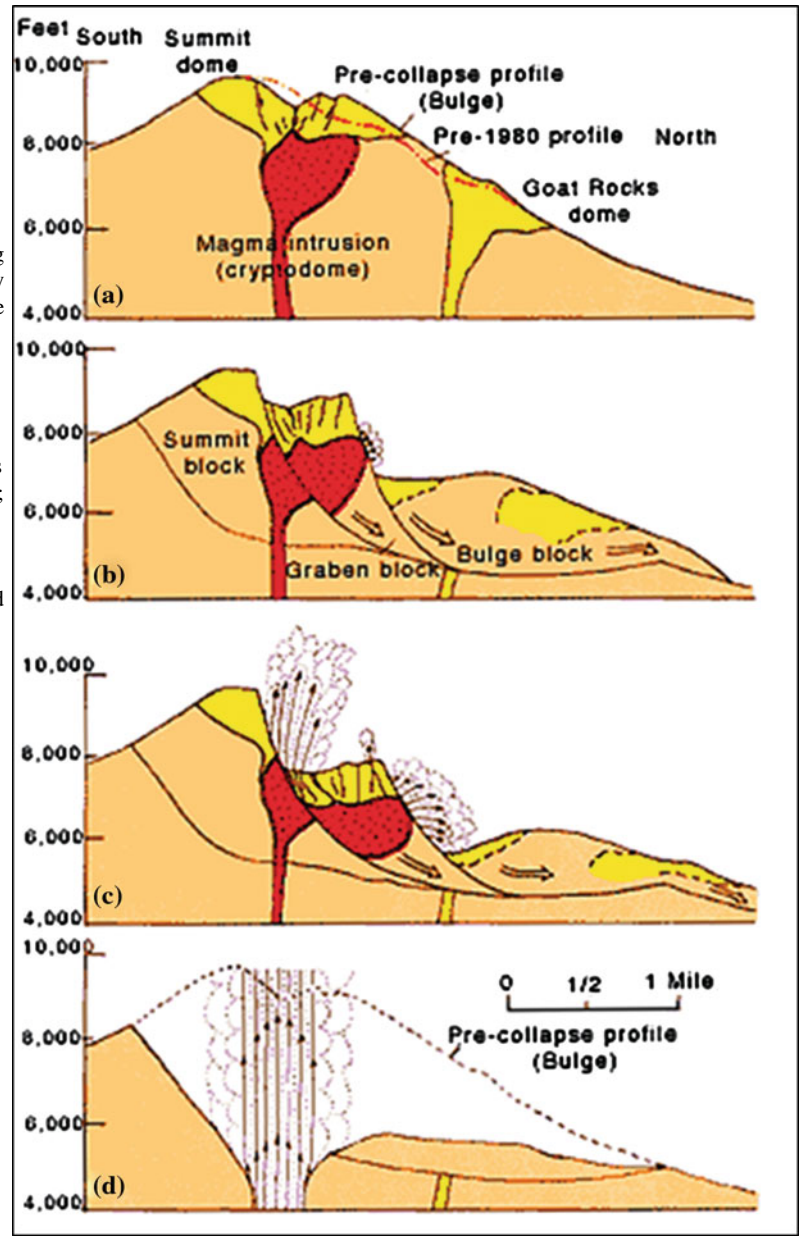

Fig. 3 Schematic cross sections of Mount St. Helens showing the cryptodome of magma that produced the bulge and the three major blocks that collapsed retrogressively to form the debris avalanche. **a** The volcano in the early morning of May 18, 1980; the bulging of the north flank is shown by the pre-1980 and pre-collapse profiles. **b** and **c** (within 30 s after the collapse) shows the progressive development of the debris avalanche and the beginning of both the lateral blast and vertical eruption, as the cryptodome was exposed; the Bulge block was the first to slide, followed by the Graben block. **d** (30 s later), by now the Summit block had slid and the lateral blast had stopped; the vertical eruption was now in full fury. After USGS Professional Paper 1250, courtesy of USGS

the northern flank had grown outward about 140 m at consistent rates of about 2 m per day and was creeping more rapidly toward failure.

At 8:32 a.m. on May 18, 1980, a magnitude 5.1 earthquake triggered the volcano's northern bulge and summit to fail and slide away as a huge landslide, first as slide blocks that quickly transformed into a debris avalanche (Fig. 3b). The debris avalanche swept around and up bedrock ridges as far as 8 km north of the volcano crater, but most of it turned westward and flowed 25 km down the valley of the North Fork Toutle River (Fig. 4) and formed a hummocky deposit (see Fig. 1). The initial slide masses accelerated to an average of 45 m/s 10 s after detachment and increased to 70–80 m/s during the following 10 s. The avalanche flow, with maximum velocities around 90 m/s, took about 10 min to travel the

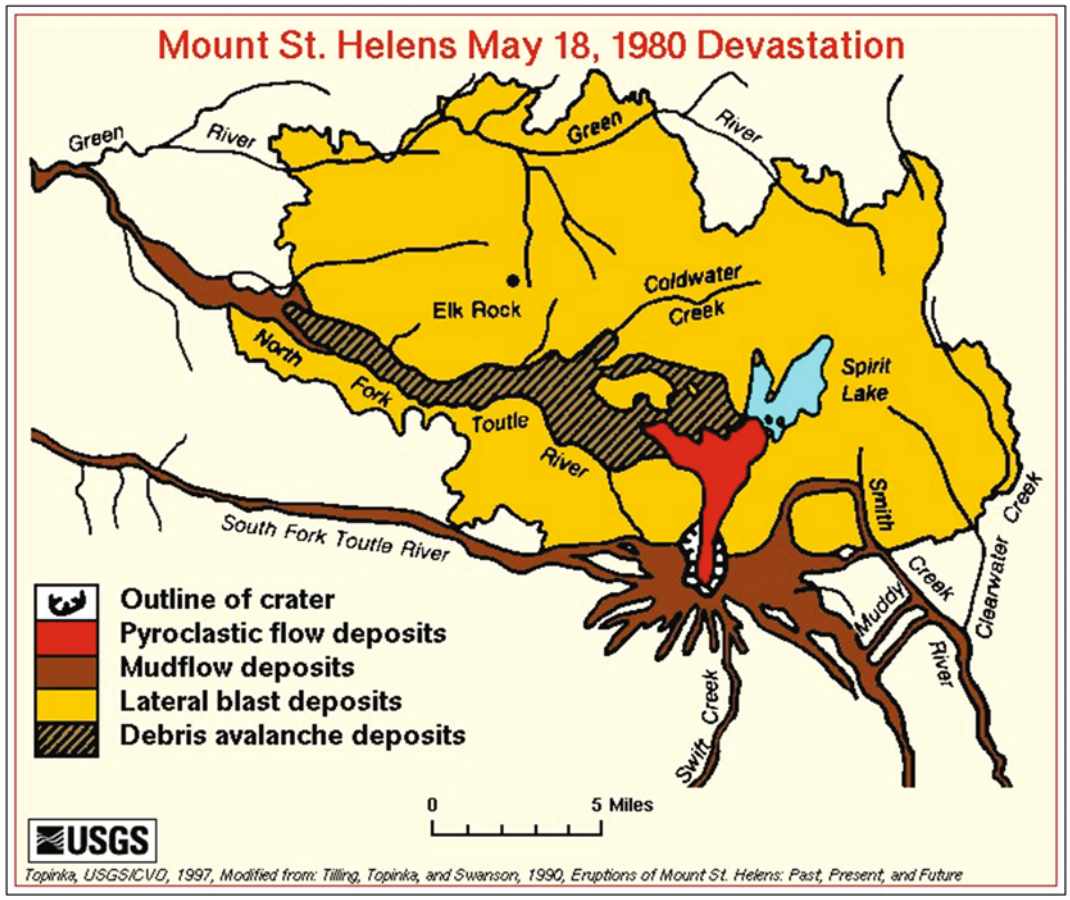

Fig. 4 Generalized geologic map showing the impact and deposits of the climatic eruption in the vicinity of Mount St. Helens volcano. Courtesy of USGS

25 km down the Toutle River (Voight et al. 1981). About 60 km^2 of the North Fork Toutle River valley system was choked with avalanche debris to an average depth of 45 m.

The landslide removed Mount St. Helens' northern flank, resulting in immediate depressurization of the volcano's magmatic system and triggering a powerful magmatic explosion that blasted laterally through the sliding debris (Fig. 3c). This directed blast consisted of hot juvenile material, the initial volcanic unit of May 18, that accelerated to at least 480 km/hr and overtook the debris avalanche and created a 600 km^2 blast zone that devastated the forest and blanketed it with a deposit of hot debris for as far as 25 km north and northwest of the crater (Hoblitt et al. 1981). With this release of pressure on the volcano's plumbing system (Fig. 3d), which caused a depressurization wave to propagate down the conduit to the subsurface magma reservoir, a 9-h long Plinian eruption immediately followed, with its huge vertical eruption plume and by far the largest of the six 1980 pyroclastic-flow events (Rowley et al. 1981, 1985; Kuntz et al. 1990).

During the first few minutes of the eruption, parts of the blast cloud and pyroclastic flows surged over the crater rim and down the west, south, and east sides of the volcano and quickly eroded and melted the snow and ice on the volcano, creating surges of water that eroded and mixed with loose rock debris so as to form lahars

that poured down the volcano into river valleys, ripping up trees and destroying roads and bridges (see Fig. 4). The largest and most destructive debris flow occurred in the North Fork Toutle River after the debris avalanche came to a halt and some of the material was remobilized hours later. The debris flow that formed by water (originally groundwater and melting blocks of glacier ice) escaping from inside the avalanche deposit through most of the day, created a powerful slurry that eroded material from both the landslide deposit and from the channel bed of the North Fork Toutle River. The debris flow increased in size as it traveled downstream, eventually reaching its maximum size at about 80 km downstream from the volcano (Voight et al. 1981, 1983; Glicken 1998).

3 Collapse Styles in Volcanic Terrains

Sources of structural collapse leading to volcanic landslides have typically been recognized as the "volcano type" similar to that described from Mount St. Helens. However, other volcanic landform collapse types have been recognized in the geologic past that produced similar volcanic landslides (e.g., Mackin 1960; Hacker et al. 2002, 2014; Rowley et al. 2006; Biek et al. 2015). These include the collapse of growing laccoliths not associated with volcano edifice intrusions, as well as collapse of large portions of the volcanic field itself during volcanic buildup (Fig. 5). Nomenclature varies widely on the use of the terms flank versus sector collapses within the "volcano" literature. Flank collapses do not usually involve the magmatic conduit, while sector collapses do, and usually involve taking most of the volcano summit off in the process. In the broadest meaning, a sector collapse is defined as a gravity-driven movement of a portion of a volcano, independent of its size, origin, and type (Acocella 2005). Flank collapses would then fall within the definition of a sector collapse. Without introducing new nomenclature to collapses produced from laccoliths and volcanic fields, we have adopted the volcano collapse terminology for all three (volcano, laccolith, and volcanic field) collapse types.

Smaller-scale failures are here referred to as flank collapses that mostly produce debris avalanche deposits from shallow slope failures (Fig. 5). The larger-scale failures are referred to as sector collapses and involve larger sections of a volcanoes' or volcanic field's substrate, or a laccolith's laterally buttressed country-rock area. With this usage, sector collapses from the three collapse types involve movement along deep-seated failure surfaces where the displaced mass laterally ramps onto the land surface and takes on the geometry of an extensional looking "thrust fault" complete with a bedding-plane fault (younger on older strata), ramp fault, and former land-surface fault (older on younger strata).

3.1 Volcano Collapse Type

Structural slope failures at volcanoes are the most recognized and studied of the three collapse types (see Fig. 5). Once considered rare, volcanic collapse is now recognized to be a common process in the evolution of volcanoes. Landslides from volcanoes occur in many different settings and scales, independent of their composition (mafic and silicic), shape (cinder cones, stratovolcanoes, and shield volcanoes), and geodynamic setting (divergent and convergent margins, hot spots). Volcanic edifices are the result of the repeated emplacement, usually within time spans of many thousands of years, of magmatic products in a limited area. As a consequence of this relatively rapid construction, any volcanic edifice with significant height can become unstable and fail.

Structural failure at large volcanoes may be confined to a volcano flank, or may involve a large portion of the edifice (sector collapse). Besides Mount St. Helens, there are several well-known examples of volcanic landslides during the twentieth century such as Bezymianny (Gorshkov 1959; Belousov 1996), Shiveluch (Gorshkov and Dubik 1970; Belousov 1995), and the Soufriere Hills volcano in Montserrat

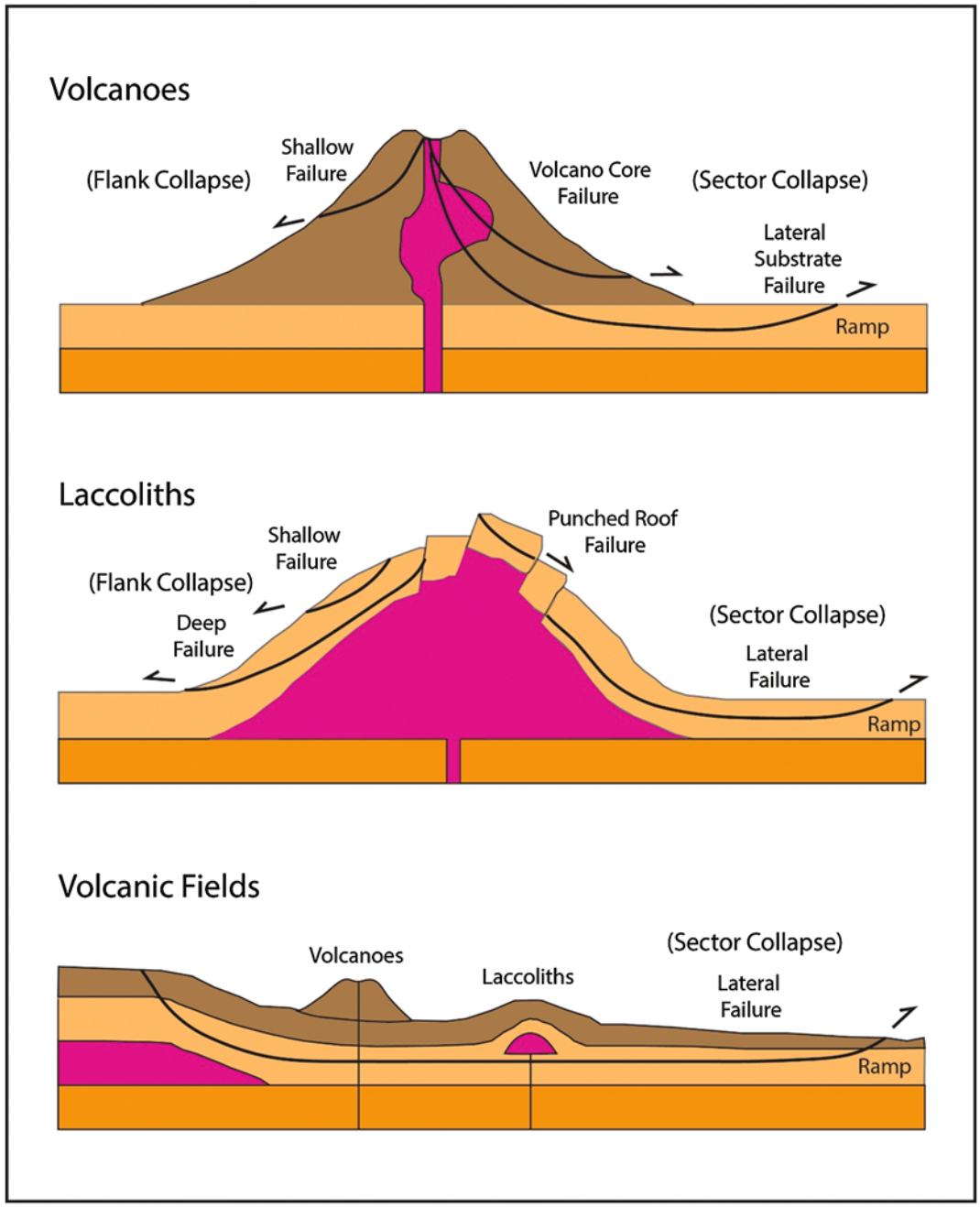

Fig. 5 Schematic diagram of collapse styles associated with volcanoes, laccoliths, and volcanic fields. Upper volcanoes diagram modified from van Wyk de Vries and Delcamp (2015)

(Voight et al. 2002). Sector collapses from volcanoes have also produced very large prehistoric subaerial landslides: the 2200 km^2, 22–33 km^3 Nevado de Colima event, Mexico (Stoopes and Sheridan 1992); the 500 km^2, 36 km^3 Socompa event, Chile (van Wyk de Vries et al. 2001); the 990 and 1200 km^2, ~30 km^3 Barú events, Panama (Herrick et al. 2013), and the 450 km^2,

26 km^3 Mt. Shasta event, USA (Crandell et al. 1984).

Volcano-generated landslides generally range in size from less than 1 km^3 to more than 100 km^3. The high velocity and great momentum of landslides allows them to cross valley divides and run up slopes several hundred meters high, as at Mount St. Helens where its 2.5 km^3 landslide reached speeds of 50–80 m/s and surged up and over a 400 m high ridge located about 5 km from the cone. Another remarkable feature derived from volcanic sector collapses of volcanoes is the source area. Because most large volcanic landslides remove the summit of the failed volcano, a horseshoe-shaped crater or semi-amphitheater is formed that varies in size based on the volume of the removed slide, typically from more than 1 km^3 up to several tens of km^3 (Carrasco-Núñez et al. 2011).

By removing a large portion of a volcano's cone, a landslide may abruptly decrease pressure on the shallow magmatic and hydrothermal systems, which can generate explosions ranging from a small steam explosion to large steam and magma driven directed blasts. These result in tephra and ash-fall-tuff hazards for surrounding areas. Collapse events can be grouped into three types: those involving a magmatic eruption, those involving non-magmatic explosions, and those that are 'cold' and have no volcanic activity associated with them (Siebert 1984; Carrasco-Núñez et al. 2011). The first type is called a *Bezymianny*-type, which refers to the magmatic eruption and collapse of the Bezymianny volcano in Russia in 1956 similar to Mount St. Helens, where magma intruded the cone and destabilized the flank. The second is called a *Bandai*-type, which refers to the Bandai volcano in Japan, whose flank collapsed in 1888 and produced a phreatic eruption. In this case, magma did not intrude the cone and the collapse depressurized an active hydrothermal system, producing vigorous phreatic eruptions without magma reaching the surface. The third type is generally referred to as an *Unzen*-type after a sector collapse in Japan occurred in 1792 but did not involve any volcanic activity.

3.2 Laccolith Collapse Type

Historic growth of laccoliths in volcanic fields has been observed in the form of cryptodome growth in the landscape surrounding volcanoes, such as the classic growth of the Showa-Shinzan dome in Japan in the mid-1940s (Yokoyama 2002). A postmaster, Masao Minatsu, in a nearby village documented its growth by drawing its slowly changing shape on a paper window of his office. He showed that over a years' time (from August 1944 to September 1945) magma caused the 100 m thick sedimentary cover to be uplifted over 200 m. The top of the roof contained a punched section that continued to rise like a piston above the main dome, yet the roof did not collapse to trigger a volcanic eruption.

The idea of volcanic landslides generated from laccoliths was first described by J. Hoover Mackin, who showed that laccoliths can produce large landslides (Mackin used the term gravity slide) on the scale of collapsing volcanoes during the vertical growth of the laccolith (Fig. 6; Mackin 1960). Laccolith intrusions "make room" for themselves in the shallow crust and thus must deform and inflate the surface considerably, in places producing steep unstable slopes. Most of the instructive field studies of laccoliths have been made where erosion has stripped most of the cover and surrounding strata to expose their intrusive cores. Therefore, most evidence of volcanic landsliding has been eroded from the record of most exposed laccoliths. However, studies from laccoliths in the Iron Axis magmatic province in southwestern Utah have revealed evidence of multiple collapse structures that led to volcanic landsliding as well as to initiation of volcanic eruptions (Fig. 5; Hacker et al. 2002, 2007; Rowley et al. 2006; Biek et al. 2009).

The Iron Axis laccolith group consists of a series of lower Miocene calc-alkaline hypabyssal laccoliths and associated volcanic rocks located just west of the present Colorado Plateau (Fig. 7). During Iron Axis magmatic activity, ascending quartz monzonite to granodiorite porphyry magma from a deep batholith complex intruded along one or more northeast-striking,

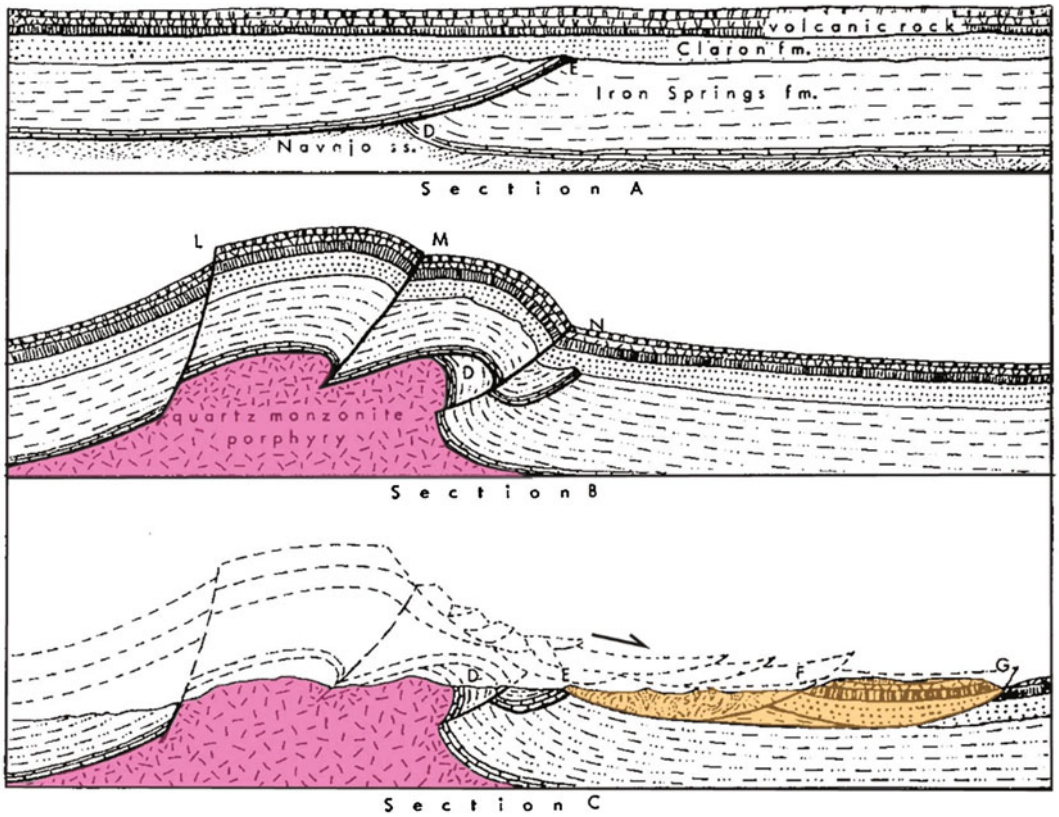

Fig. 6 Structural features associated with the Iron Mountain laccolith, Iron Axis, Utah. **a** Restoration of pre-intrusive structure showing east verging Cretaceous Sevier thrust sheet eroded and unconformably overlain by Tertiary sedimentary and volcanic strata. **b** Restoration after emplacement of Iron Mountain intrusion along former thrust fault and vertical inflation. **c** Same as **b** but showing gravity slides (remaining erosional remnants colored) formed by collapse of oversteepened eastern flank. Modified from Mackin (1960)

east-verging Cretaceous Sevier thrust faults before being emplaced as bulbous laccoliths within Mesozoic and Tertiary sedimentary rock units (Mackin 1960; Blank and Mackin 1967; Blank et al. 1992; Rowley et al. 1998; Rowley 1998). More than a dozen exposed intrusions have been mapped within the magmatic province and others are inferred from structures in the roof rock, geophysical data, and drilling (Rowley et al. 2006; Biek et al. 2009). The intrusions occur in a northeast-trending belt that follows the trend of the Sevier orogenic front. The intrusions were forcibly emplaced into sedimentary rocks at depths ranging mostly between 2.5 and 0.25 km and deformed their roofs by upward folding and faulting.

Detailed studies show that the laccoliths in the Iron Axis form a continuum from sill injection to domed laccolith structures through a rapid incremental, or even a single-pulse growth (Hacker 1998; Hacker et al. 2002, 2007; Petronis et al. 2004). Structural and topographic relief produced by the emplacement of laccoliths progressed in stages, beginning with initial sill formation that was either laterally fed by transport of magma along pre-laccolith thrust faults or vertically through feeder dikes, followed by subsequent inflation of the sill by forcible intrusion of continuous or multi pulses of magma (Fig. 8). Bending of the entire roof overburden began as magma was continually added to the base of the laccoliths to forcibly thicken the intrusions

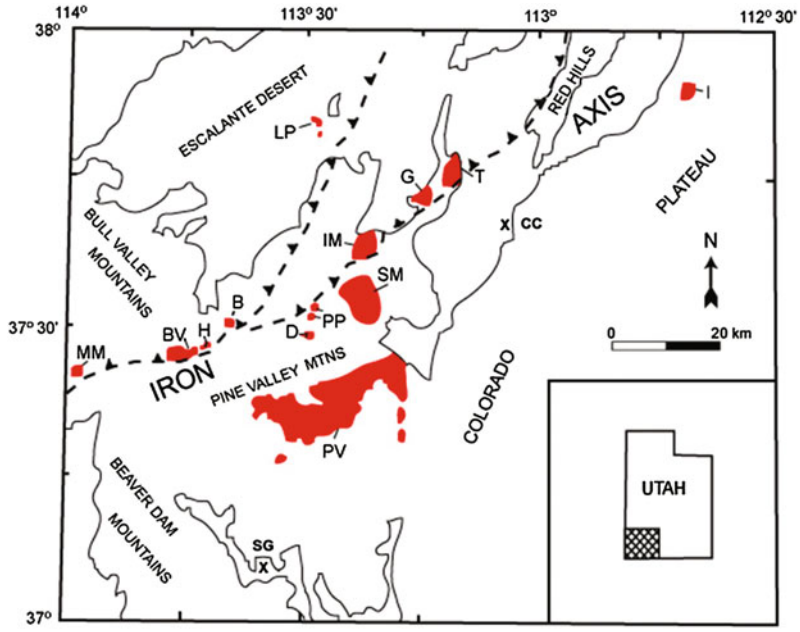

Fig. 7 Map of southwest Utah, USA, showing intrusions of the Iron Axis magmatic province: *B*—Big Mountain; *BV*—Bull Valley; *D*—The Dairy; *G*—Granite Mountain; *H*—Hardscrabble Hollow; *I*—Iron Peak; *IM*—Iron Mountain; *LP*—Lookout Point; *MM*—Mineral mountain; *PP*—Pinto Peak; *PV*—Pine Valley; *SM*—Stoddard Mountain; *T*—Three Peaks. General trend of Sevier age thrust faults shown as dashed lines with saw-teeth. Towns: *CC*—Cedar City; *SG*—St. George. Modified from Hacker et al. (2007)

vertically. As intrusions inflated, the overlying host rocks were gently rotated and arched into doubly hinged flexures around the periphery. Due to the shallow emplacement (thin overburden), extension over the up-arched area was accommodated by brittle fracturing and high-angle reverse and normal faulting of the roofs. The geometry of most laterally fed laccoliths is asymmetrical in cross section, with the over-steepened flank of the laccolith occurring on the side farthest from the source area (to the east), which corresponds to where the sill stopped. Thus the laccolith is thickest where magma piled up, so to speak, from continued lateral injections.

The unusual aspect of laccolith growth in the Iron Axis group is the catastrophic structural collapse of some of the laccoliths flanks and roofs and subsequent venting of pyroclastic flows (ash flows) and lava flows. As the concordant intrusions continued their vertical growth, the limbs of the overlying peripheral flexure steepened as the hinges tightened. Extensional faulting at the hinge crest most likely reduced the lateral support of the limb on an otherwise already steepened and unstable slope. The resulting slabs of host rock detached within shale units of the sedimentary rocks and slid onto the former land surface below (see Hacker et al. 2002, 2007). The sudden loss of peripheral overburden greatly reduced the lithostatic pressure that was essentially holding the roof "down" in advance of the upward loading forces applied by the thickening magma. This sudden release of overburden by sliding most likely resulted in immediate frothing of the magma due to massive pressure release, as with the 1980 Mount St. Helens eruptions (Lipman and Mullineaux 1981).

Field evidence clearly shows that intrusive doming produced by the growing laccoliths created unstable slopes from which large segments of host rock material were catastrophically sloughed by sliding prior to volcanic eruptions. This sequence of events (i.e., doming, then gravity sliding, then volcanism) indicates that volcanism

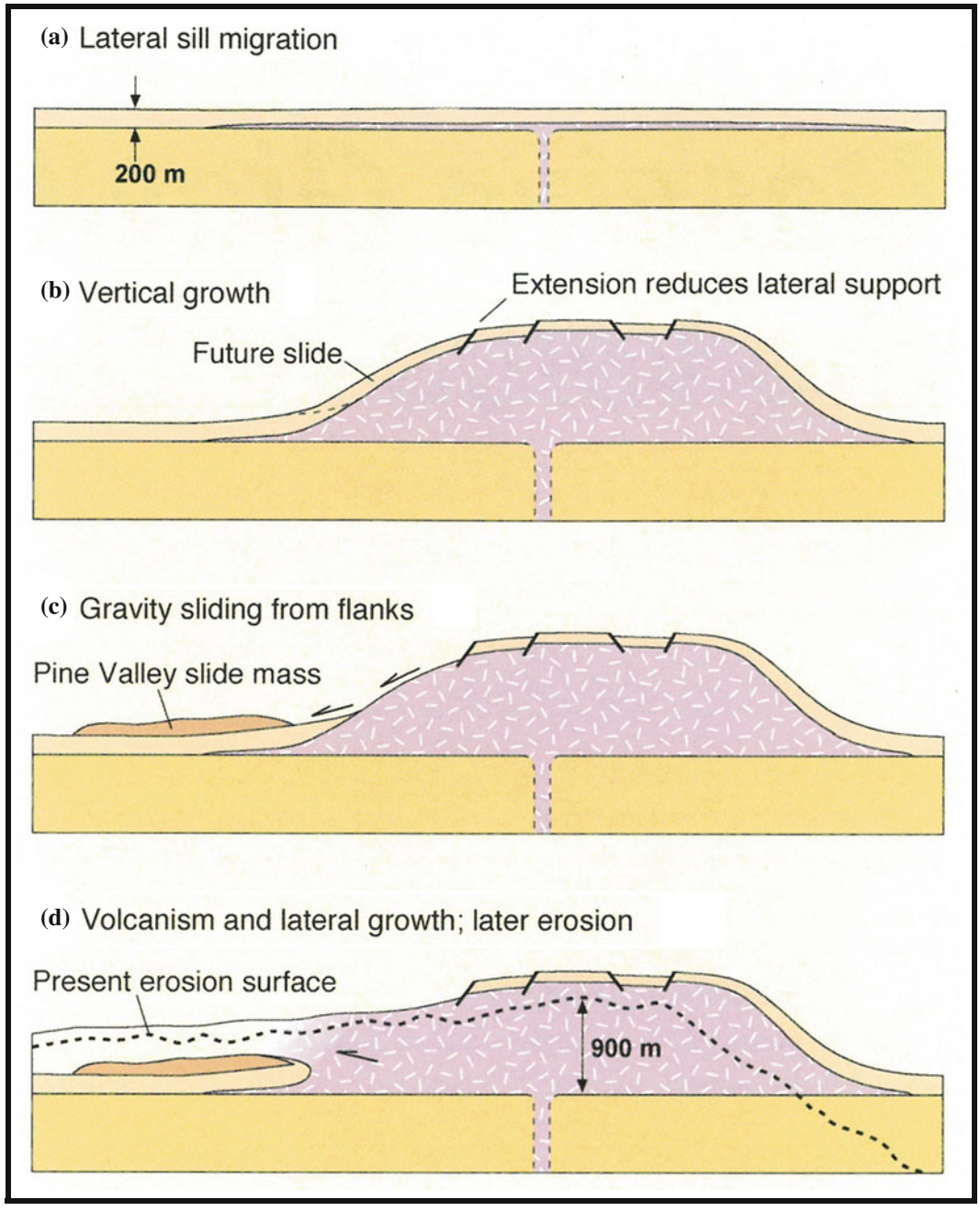

Fig. 8 Schematic model for evolution of laccoliths in Iron Axis using the Pine Valley laccolith as a proxy. Cross-section is north-south through laccolith. Emplacement and growth is envisioned to be a continuum from one stage to the next. **a** Stage 1—ascent of magma through en echelon dike system followed by lateral migration of sill to its fullest extent. **b** Stage 2—vertical laccolith growth by continued sill emplacements at the base of the intrusion. **c** Stage 3—gravity sliding from laccolith by flank failure and continued growth. **d** Stage 4—volcanic eruptions of pyroclastic flows (or in the case of the Pine Valley laccolith, lava flows) onto the landslide and surrounding surface, followed by continued lateral laccolith growth. Modified from Hacker et al. (2007), courtesy of Utah Geological Survey

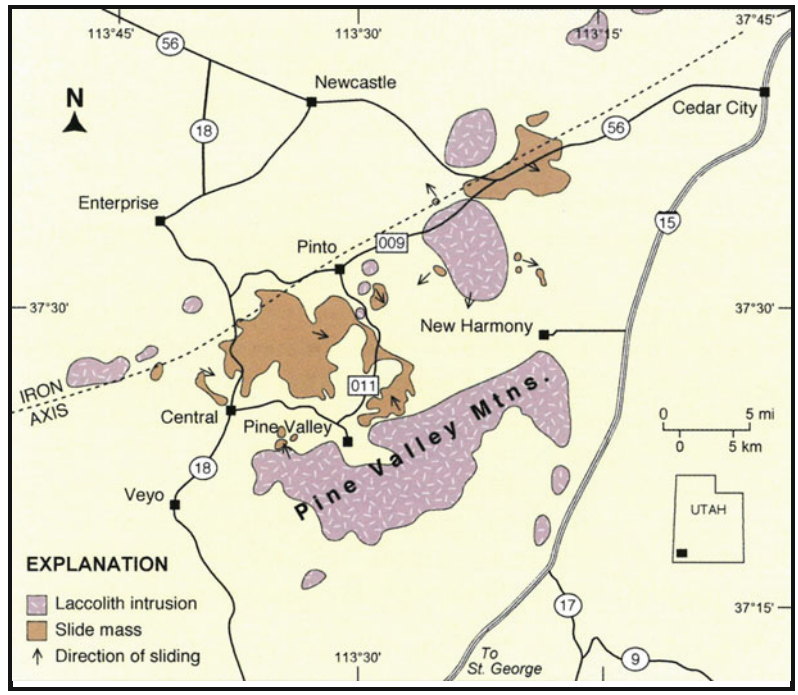

Fig. 9 Laccolith intrusions and slide masses within the central area of the Iron Axis. *Arrows* indicate primary direction of slide movement away from source intrusion. Largest slide mass is the Big Mountain slide. Modified from Hacker et al. (2002), courtesy of Utah Geological Survey

was initiated by gravity sliding. At least seven major collapse episodes in the Iron Axis can be attributed to the rapid emplacement of laccoliths (Lookout Point, Pinto Peak, Bull Valley-Big Mountain, Iron Mountain, Stoddard Mountain, and Pine Valley; Fig. 7) with at least five (Pinto Peak, Bull Valley-Big Mountain, Stoddard Mountain, and Pine Valley) triggering a volcanic eruption event (Blank et al. 1992; Hacker 1998; Hacker et al. 1996, 2002, 2007). The volcanic landslides were generated by three types of slope failure (Fig. 5): (1) flank failure where sedimentary host rocks failed on the over-steepened slopes of the laccolith, (2) punched roof failure where large block sections of the host-rock were faulted upward in piston fashion by the magma to the point that they lost lateral support and failed, and (3) sector collapse where a thicker section of the laccolith's flank and surrounding buttressed sedimentary strata failed laterally away from the laccolith (similar to the substrate failure type of volcanoes). Most of the volcanic landslides generated were composed of slides, with minor portions of the debris-avalanche component occurring in more distal regions.

The largest slide mass (Big Mountain event), with a volume of ~50 to 60 km^3, covers >150 km^2, is more than 550 m thick in places and it extends more than 25 km from its parent laccolith dome (Figs. 9 and 10). The Big Mountain event represents a sector collapse type, which makes this laccolith collapse event larger than the Mount St. Helens volcano event.

The transported stratigraphic units within slide masses show attenuation and exhibit various internal structural complexities; however, normal internal stratigraphic succession is maintained. Typically, the strata exhibit pervasive internal fracturing and shattering but are well indurated. Some members and formations are brecciated and consist of pebble-to-boulder-sized, angular to subangular rock fragments with a crushed matrix of the same composition as the fragments (Fig. 11). The brecciated zones are commonly matrix-poor, with the fragments commonly tightly packed in a jigsaw-puzzle mosaic separated by a cataclastically generated sand-to-granule-size matrix. Most fragments have moved slightly relative to their neighbors, while others show some rotation. Rocks from adjacent

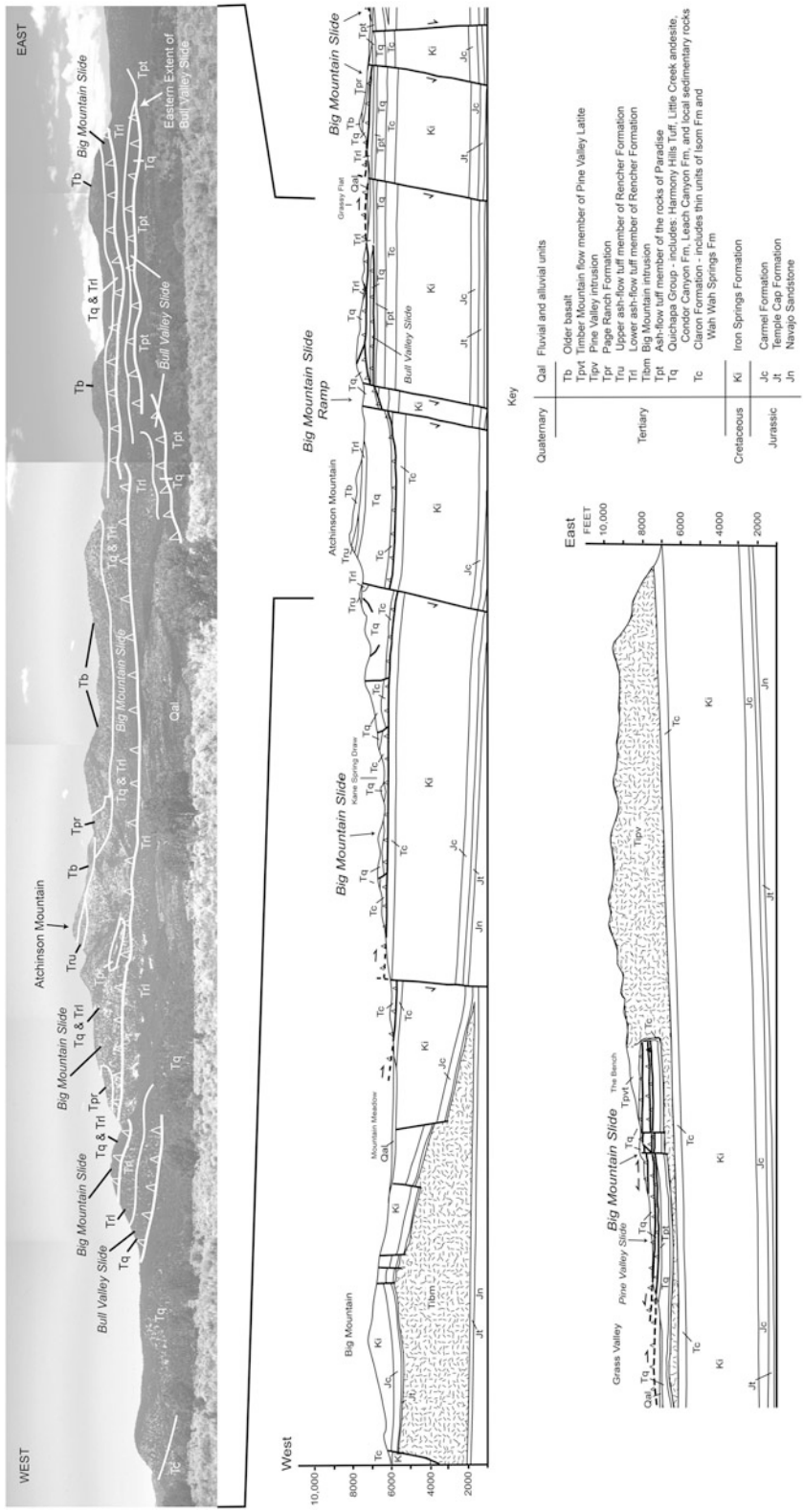

Fig. 10 Geologic cross section (east-west) through the Big Mountain gravity slide showing the ramp just to the east of Atchinson Mountain. Modified from Hacker et al. (2002)

Fig. 11 Outcrop of pre-collapse welded tuff exhibiting pervasive internal fracturing with angular to subrounded fragments in a crushed matrix formed during slide transport within Bull Valley gravity slide

stratigraphic units are usually not mixed, but locally are chaotically juxtaposed along close-spaced shear domains. Omission or smearing out of stratigraphic units takes place along low-angle shear zones or bedding-plane faults. Mechanically, the character of the internal deformation varies with rock lithology. Softer, moderately welded ash-flow tuffs deformed along sheared zones as much as 3 cm thick that contain pulverized rock flour material (cataclasite) formed by the mechanical breakdown by crushing and grinding of the tuff. In contrast, the more competent highly welded tuffs and lava flows deformed along brittle intersecting or anastomosing sets of shear fractures, which resulted in brecciation of the rocks. In addition to internal deformation fabrics of the rock units, many structurally complex areas within the slide masses contain extensively faulted and folded strata. Faulting occurs along: (1) local tear faults oriented parallel to transport direction, and (2) high-to low-angle normal and reverse faults oriented mostly perpendicular to transport direction.

Overall, the slide masses closely resemble remnants of "erosional thrust sheets" in form. All deformation is confined to the slide masses themselves and abruptly terminates downward at low-angle, basal-bounding gravity-slide faults (analogous to attenuation or denudation faults or to non-rooted detachment faults). The basal gravity-slide faults are a composite of four types of fault surfaces. They include: (1) a subhorizontal "bedding fault" (decollement) within shale-rich sedimentary rocks in which younger rocks overlie older rocks, (2) subvertical "flanking faults," which are lateral bounding tear faults with strike-slip movement, (3) a transgressive "ramp fault" that cuts upward across bedding, and (4) a subhorizontal "land surface fault," which is a fault between the slide mass and the pre-existing land surface of that time, in which older rocks overlie younger rocks. All four fault components are not necessarily preserved beneath every slide mass due to differential erosion, especially at the promixal ends of the slide masses where the bedding and ramp structures were mostly located at higher elevations on the intrusive domes and therefore were more susceptible to erosion. Alternatively, some of the components were destroyed by subsequent extrusion of magma. The Big Mountain slide is the most complete structure, for it retains a set of all four bounding faults (see Fig. 15 for illustration of fault types).

The relationship of gravity sliding as triggers for volcanic eruptions is evident in the Iron Axis laccoliths. The areas of structural and topographic relief that were necessary for the formation of gravity slide structures were formed by the forceful intrusion of quartz monzonite magma into sedimentary rocks and structurally uplifting these host rocks by laccoliths. The close timing between sliding and volcanism suggests that eruptions from the laccoliths could not take place until the initiation of gravity sliding. Sloughing off part of the roof of some of the laccoliths reduced the overburden pressure on the magma, leading to violent magma frothing

(vesiculation) and explosive eruptions. Most initial volcanic activity was of the pyroclastic flow type. The pyroclastic flows traveled laterally outward over the landscape in the direction of the slide movement, immediately burying most of the slide deposits and surrounding landscape. The largest pyroclastic deposit covered an area of >1000 km^2. The volumes of the volcanic deposits do not appear to correspond to the size of the collapse features, that is, the smallest of failures (the punched roof block failure) could release enough pressure to initiate the same size eruption as the larger lateral failure.

3.3 Volcanic Field Collapse Type

Volcanic field collapses are the supervolcanoes (e.g., Yellowstone caldera type eruptions) of the volcanic landslide world. Although these volcanic field collapses are rare and the least recognized, due in part to the lack of modern analogs, they have formed the largest subaerial volcanic landslides on Earth (Hacker et al. 2014; Biek et al. 2015). This type of collapse involves shear failure along a large portion of the substrate of a volcanic terrain, resulting in mass movement of gigantic sections of the volcanic field (a mega-sector collapse). Collapse of a volcanic field can incorporate not only multiple volcanoes, but also shallow or older stocks, laccoliths, sills, and dikes, as well as any volcanic landform associated with the field's evolution (Fig. 5).

A volcanic field is an area of the Earth's crust that is prone to localized volcanic activity and generally contains numerous volcanoes of either the monogenetic or polygenetic type. A polygenetic volcanic field contains polygenetic vents, each of which erupts repeatedly over long periods of time. Unlike monogenetic volcanoes, polygenetic volcanoes reach massive sizes, such as Mauna Loa, which is the world's largest active volcano. Polygenetic volcanoes include stratovolcanoes, complex volcanoes, shield volcanoes and calderas. The Marysvale volcanic field is a polygenetic field located in southwestern Utah and is one of the largest volcanic fields in the western United States (Rowley et al. 1998, 2002, 2005). Most of its volcanism took place from early Oligocene to late Miocene (about 32 to 14 Ma).

Partial collapse of the southwestern part of the Marysvale volcanic field produced a volcanic landslide, the Markagunt gravity slide, with an areal extent of at least 5000 km^2 (dimensions revised from Hacker et al. 2014), making it the largest known subaerial gravity slide on Earth. It is larger than the famous 3400 km^2 Heart Mountain gravity slide of Eocene age in the Absaroka volcanic field of northwestern Wyoming, long considered to be the largest subaerial landslide (e.g., Malone and Craddock 2008; Beutner and Hauge 2009; Craddock et al. 2009). The Markagunt gravity slide took place at about 21.5 Ma, prior to basin-range tectonism. Basin-range faulting, which produced north-trending basins and ranges that form the present topography, overprinted those structures formed during gravity sliding. Nonetheless, grooves, striations, Riedel shears, pseudotachylyte (Fig. 12), crushed and rehealed clasts, basal cataclastic breccia, and clastic dikes that we have identified provide strong evidence of southward catastrophic emplacement by gravity slid-ing. The uniformity of directional indicators, the stratigraphic sequence of volcanic rocks that make up upper-plate strata, and the overall geometry of the gravity slide show that it represents a single emplacement event (Biek et al. 2014, 2015; Hacker et al. 2014).

From its mapped breakaway zone in the central Tushar Moun-tains and central Mineral Mountains to the southern limit of its debris avalanche deposits in the northern Markagunt Plateau and eastern Black Mountains, the gravity slide is presently about 95 km long and at least 65 km wide at the latitude of the ramp (Fig. 13). Southward transport after the ramp of at least 32 km occurred over the former Miocene land surface. The southwestern part of the Marysvale volcanic field, which consists of clustered stratovolcanoes and subordinate yet important calderas, is built on a weak substrate of mostly fine-grained volcaniclastic strata of the Brian Head Formation, which to this day are famously prone to modern landsliding. We remain uncertain what triggered the giant gravity slide, but

Fig. 12 *Upper image* Pseudotachylyte on secondary shear plane along sharp contact between highly fractured sandstone of the Bear Valley Formation below and volcanic deposits of the Mount Dutton Formation above. *Lower image* close-up of pseudotachylyte-filled dike injected downward into sandstone at GPS receiver in center of photo

suggest that it was triggered by pre-caldera inflation of the 20–18 Ma Mount Belknap caldera (Fig. 14) or perhaps by earthquakes associated with this inflation.

At its simplest form, the gravity slide is a great sheet of volcanic rock that slid many km southward and at its distal southern end placed older rock on younger rock above a

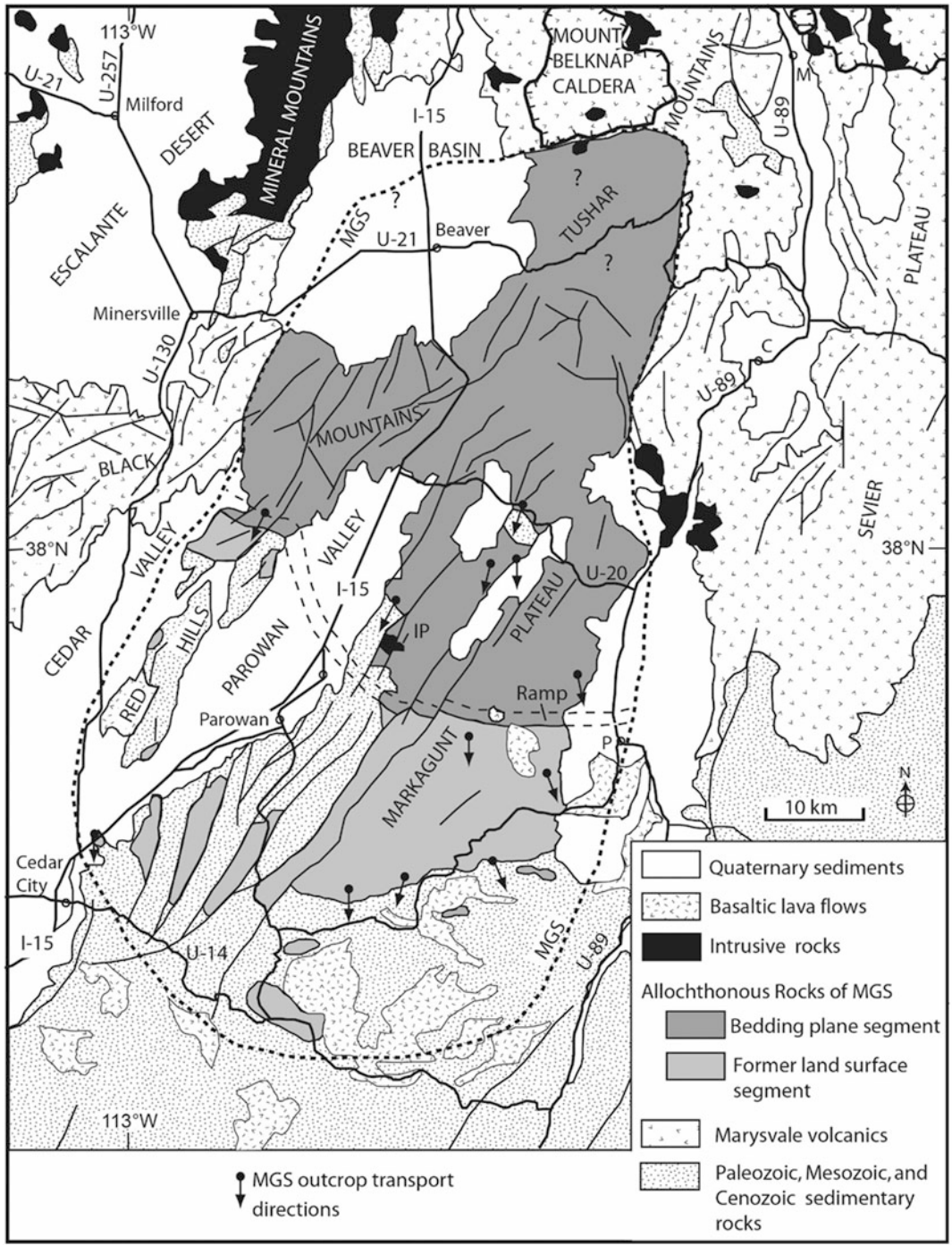

Fig. 13 Simplified geologic map showing extent (*heavy dashed line*) and features of the Markagunt gravity slide (MGS). *C* Circleville; *IP* Iron Peak intrusion; *M* Marysvale; *P* Panguitch. Modified from Hacker et al. (2014)

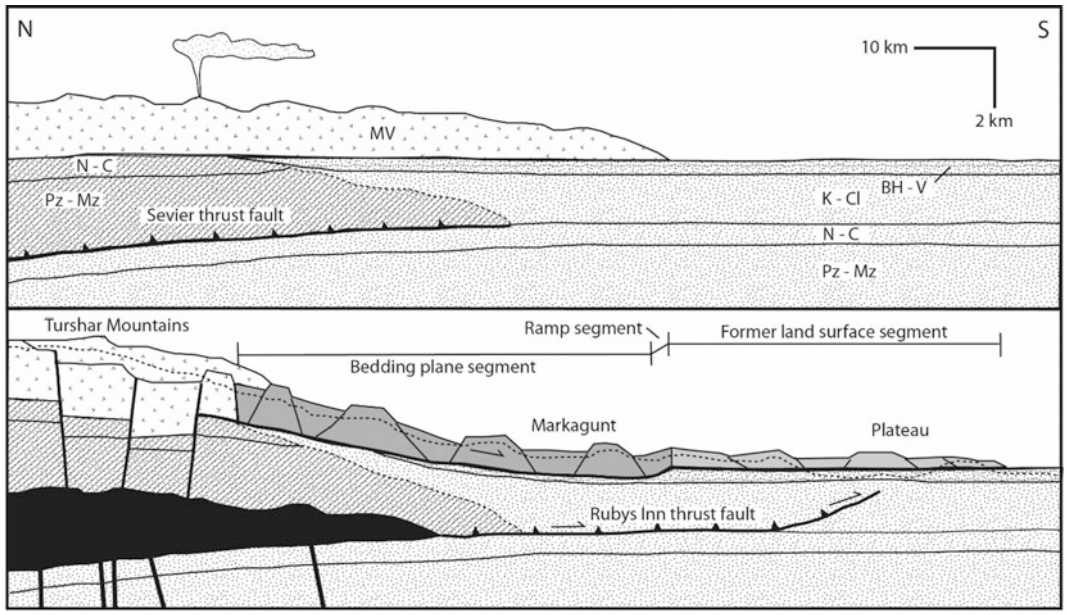

Fig. 14 Diagramatic N-S cross section of Markagunt gravity slide before and after sliding; Although interpretive (based on cross sections using petroleum exploration wells), late-stage intrusions (area shown in *black* in lower cross section) utilized Sevier thrust faults, doming the overlying volcanic field. Pz-Mz, Paleozoic and Mesozoic sedimentary rocks; N-C, Jurassic Navajo Sandstone and Carmel Formation; K-CL, Cretaceous and Claron Formation sedimentary rocks; BH-V, Brian Head Formation and oldest regional ash-flow tuffs; MV, Marysvale volcanics. Modified from Hacker et al. (2014)

subhorizontal surface (Fig. 15). It blankets the entire central and northern Markagunt Plateau and adjacent areas and consists of large blocks many square km in size of Miocene and Oligocene regional ash-flow tuffs and local volcanic and volcaniclastic rocks (derived from the Marysvale volcanic field stratovolcanoes and calderas). One way to think of the Markagunt gravity slide is as a thick stack of playing cards representing the volcanic stratigraphy of the volcanic field that are intensely deformed along shears between individual sheets but remain relatively undisturbed in the interior of the sheet (or blocks). The fact that the gravity slide consists mostly of undeformed large blocks above the bedding plane segment, bounded below by an inconspicuous shear plane, is one of the reasons it remained undiscovered for so long. The land-surface segment, however, is structurally more chaotic and consists of large tilted blocks of volcanic rocks in a more brecciated and sheared matrix, thus representing a more debris avalanche zone of the landslide (Fig. 16).

Characteristics of these astonishingly large gravity slides suggest that these types of volcanic fields are preconditioned for gigantic displacements by virtue of their: (1) large volume of available slide material that rapidly accumulated during volcanism, creating a thick, potentially unstable wedge, (2) a possible substrate of subhorizontal sedimentary strata containing early ash from the start of volcanism that weathers to incompetent beds, (3) an underlying batholith whose growth tilts rocks outward from the center of the volcanic pile, (4) shallow intrusive complexes (mostly laccoliths and dike systems) that rose from the batholith to feed the volcanism and which add lateral stress, and (5) possible pre-collapse development of summit fractures and normal faults by intrusive doming or during gradual lateral spreading on deeper-seated thrust faults that weaken the structural integrity of the volcanic field. Recognition of these features in modern volcanic fields could aid in potential hazard assessments.

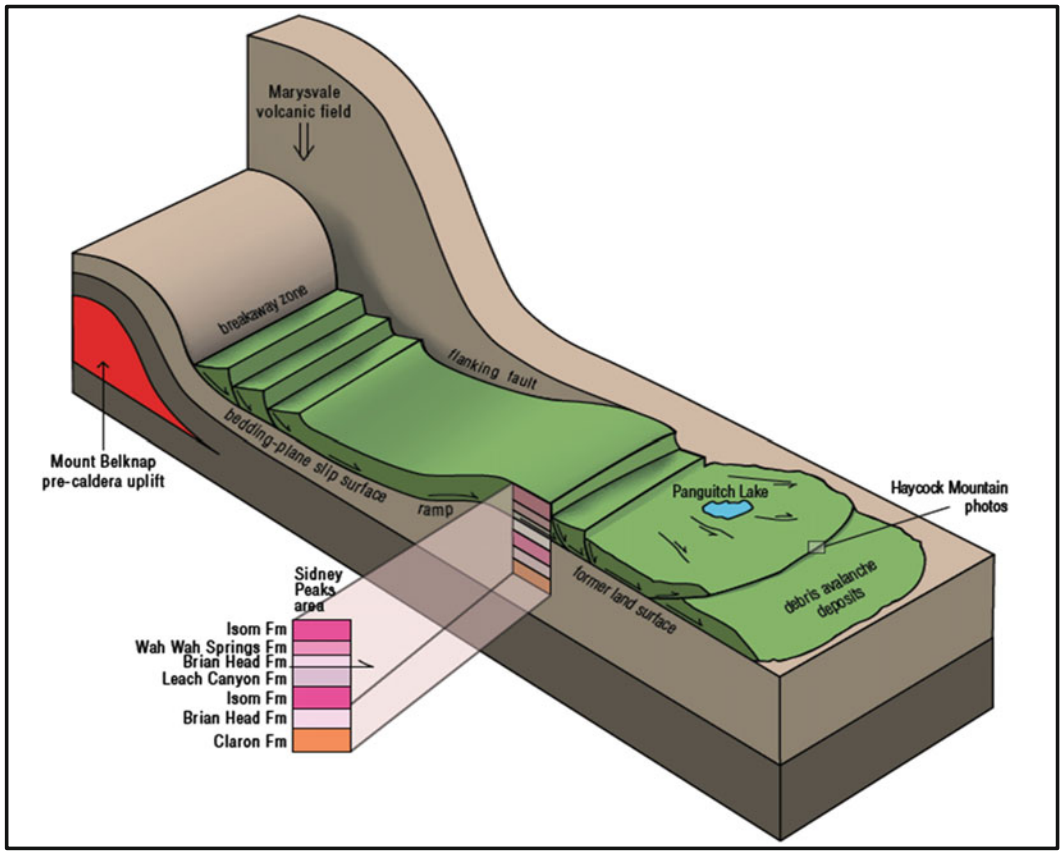

Fig. 15 Vertically exaggerated block diagram of an idealized gravity slide. Here, we suggest that the trigger is pre-caldera inflation of the Mount Belknap area, causing arching of overlying strata and consequent failure on over-steepened slopes. Note the four main bounding surfaces: the bedding-plane slip surface in mechanically weak clay-rich rocks of the Brian Head Formation; the ramp, where the slide mass breaks upward to the surface; the former land surface, now covered by the slide mass; and the flanking failure that bounds the margin of the slide. The basal slip surface resembles shallow low-angle faults, complete with slickensided and striated surfaces, cataclastic zones, local pseudotachylyte, and brittle microfabrics. Extensional deformation characterizes the upper part of the slide, whereas compressional deformation characterizes the toe area. The main part of the gravity slide remains mostly intact with individual blocks as much as several square km in size, preserving a stratigraphy inherited from the source area. Distal portions of the slide mass disaggregate into debris avalanche deposits. Because gravity is the ultimate driver of landslides, the dip of the slip surface must be sufficient such that the downslope component of the weight of the slide mass overcomes the frictional resistance to sliding at the detachment layer. Once moving, however, the slides can travel many km over former land surfaces. Haycock Mountain photos shown in Figs. 16 and 18. Modified from Biek et al. (2015)

4 Volcanic Landslide Features and Deposits

Large volcanic landslides from the three main collapse types described (i.e., volcanoes, laccoliths, and volcanic fields) share a number of morphological and fabric-related features that developed during transformation of slides to debris avalanches to debris flows. Unlike individual volcanic deposits such as pyroclastic flows, recognition of prehistoric volcanic landslide deposits may be easier to identify by large-scale properties rather than by

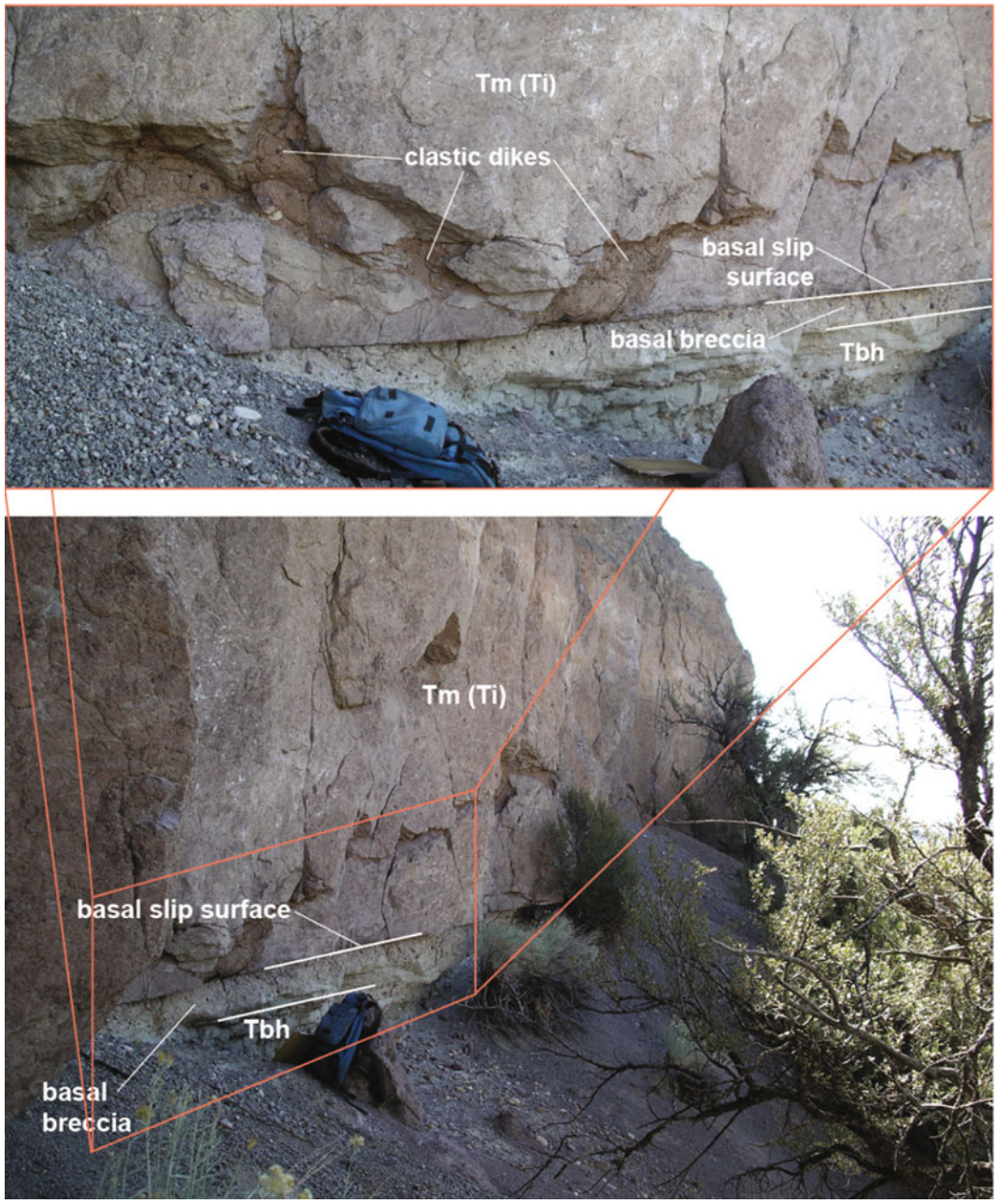

Fig. 16 Markagunt gravity slide exposure just south of Haycock Mountain. Note planar basal slip surface and underlying thin basal breccia, which in turn overlies similarly dipping volcaniclastic pebbly sandstone of the Brian Head Formation (Tbh). Basal breccia is light-reddish-brown and consists of both angular (Isom Formation) and rounded (intermediate volcanics and quartzite) clasts floating in a well-cemented sandy matrix; the breccia is texturally similar to concrete or glacial till and was derived from pulverized Isom Formation and underlying strata immediately above and below the slip surface. This breccia is injected as clastic dikes into the basal part of the gravity slide, which here consists of resistant Isom Formation (Tm[Ti]) cataclasite. This pulverized and silicified Isom Formation forms a cliff 5–10 m high and grades upward into fractured but otherwise undisturbed Isom Formation. *Inset* shows close-up of clastic dikes and cataclastic Isom Formation. Modified from Biek et al. (2014)

outcrop-scale structures or lithologies, although these are important where erosion has stripped away major portions of a slide mass.

4.1 Slide Zone

The slide zone of the three collapse types includes the area at the head of the slide mass where large slide blocks are displaced downslope as largely intact masses from the horseshoe shaped scar of the breakaway area. The large blocks are bounded by large high-angle normal faults, not only the major breakaway fault but faults that are antithetic and synthetic to it, that may form a wide variety of structures and landforms, including horsts and grabens. In edifice-scale collapses, slide blocks (toreva blocks) may show backward tilting. These high-angle faults pass into a low-angle, downslope-dipping plane or strata of weakness, especially in the case of volcanic field collapses. Typical planar surfaces in the breakaway area and downslope are disrupted by small high-angle normal and en echelon faults that strike perpendicular to the downslope direction. Most graben areas are filled in with post collapse erosional debris. This zone of the landslide is preserved only in the largest sector collapses where the landslide cuts deeply into volcanic landforms. Flank collapses are generally smaller and lack the slide blocks, so the main products preserved are debris avalanche or flow deposits. Slide-zone runout lengths vary greatly depending on the distance between the head breakaway scarp and where the slide plane daylights at the surface farther downslope, where it is a ramp fault in deep-seated collapses. Volcanic field collapses contain the largest slide zones with the Markagunt gravity slide bedding plane slip surface reaching over 60 km in length. The sides of the slide, parallel to the slide direction, represent strike-slip movement, and in the case of volcanic-field collapses may be represented by a subvertical lateral fault, much of which is a broad subvertical zone of tectonic breccia.

4.2 Debris Avalanche Zone

The surface morphology of most younger volcanic debris avalanche deposits is characterized by a hummocky terrain with numerous hills and closed depressions (Fig. 17). Hummocks (also called mounds) may form by extension as the laterally spreading avalanche produces horst and graben structures, or the hummocks may represent the surface topography of the deposit produced by avalanche blocks rafted within finer material (Voight et al. 1981, 1983; Glicken 1986, 1996; Crandell 1989). The long axis of hummocks are mostly oriented parallel or perpendicular to transport direction; some deposits contain hundreds to thousands of closely spaced hummocks. Hummock size ranges from $\sim$1 m to several hundred meters in height and >1 km in length, with height and density generally decreasing toward its distal area, reflecting progressive disintegration of internal blocks (Ui 1983; Siebert 1984, 2002; Glicken 1986, 1996; Crandell 1989). Distally, areas of flat surfaces may increase as the hummocky morphology becomes subdued and longitudinal ridges become prominent. Avalanche deposits also generally have sharply defined edges, with marginal levees and a steep terminus, although levees may be subdued or absent in avalanches that contain a higher water content.

Internally, most debris avalanche deposits are poorly sorted and poorly graded, with particle sizes ranging from silt size to extremely coarse blocks. They typically have a more bimodal fabric, consisting of a block facies and a mixed facies (also referred to as a matrix facies) (Crandell et al. 1984; Glicken 1991; Mehl and Schmincke 1999). Block (or megaclasts) dimensions range from meters to hundreds of meters in diameter and represent fragments of highly brecciated and fragmented segments of volcanic material transported relatively intact and surrounded by matrix. Block-facies material, which dominates in most hummocks, can consist of one large clast, multiple clasts of the same lithology, or multiple deformed and faulted clast

Fig. 17 The catastrophic debris avalanche at Mount Shasta showing hummocky terrain. The deposits of an exceptionally large debris avalanche extend from the base of Mount Shasta volcano northward across the floor of Shasta Valley in northern California. The debris-avalanche deposits covers an area of about 675 km^2, and their estimated volume is at least 45 km^3. Dating methods suggest that the debris avalanche occurred between about 300,000 and 380,000 years ago. (Image courtesy of USGS)

groups of different lithologies (Siebert 2002). Mixed-facies material consists of poorly sorted angular lithic fragments, in which the frequency and size of blocks decreases with increasing distance from the source and the matrix proportion rises.

Clasts in all facies are angular to subangular, highly fractured, and pervasively shattered, forming a "jigsaw" texture (both jigsaw cracked and jigsaw-fit textures) in which fragments of adjacent clasts can be visually refitted across fractures (Shreve 1968; Ui 1983). Fractured clasts of one lithology surrounded by crushed fragments of the same lithology represent the crushing of individual blocks or stratigraphic layers and are usually stretched or smeared in the direction of transport. Fracturing of crystals, glass, and lithic fragments extends to the microscopic level (Komorowski et al. 1991).

The basal region experiences high normal and shear stresses that result in intense comminution (the action of reducing a material to minute particles or fragments). Basal zones of both debris avalanches and slide zones show more penetrative shear fracturing of clasts and a smeared-out fabric of blocks, thus producing a crude layering. Pervasive shearing usually decreases in extremely short distances vertically. Clastic dikes formed by injection of matrix material into fractures during movement are commonly observed in basal regions (see Fig. 16). Basal contacts of debris avalanches show evidence of either relatively passive transport or erosive scour, as observed by lengthy contacts above largely undeformed soft sediment substrate, or striations and grooves found on substrate material or in the base of the mass (Fig. 18), along with incorporation of substrate material.

Fig. 18 Close-up of slickenlines exposed at the base of the Markagunt gravity slide at Haycock Mountain. Riedel shears and slickenlines at the base of the gravity slide demonstrate transport from north to south

Where large blocks are not present, avalanche deposits resemble angular breccias with larger clasts supported by a matrix of finer material that in most places shows evidence of intense shearing. Although a wide range of clast sizes may be present at any one location, their composition is usually not random and homogenization is far from complete. The spatial distribution of clast types reflects the original stratigraphy of the collapsing source mass, thus broad stratigraphic relationships in the source rocks are generally preserved, a fact that indicates that debris avalanche emplacement involves laminar flow rather than turbulent flow (Fig. 19).

4.3 Debris Flow Zone

Where sufficient water is present during flow, debris avalanche deposits generally grade downslope into debris flows. Such a transition has been observed at Mount St. Helens and Mount Shasta, USA, where the two types of flow deposits are distinguished on the basis of sedimentological differences (Crandell 1989). Scott et al. (2002) divide debris flows into cohesive and noncohesive types. Most debris flows contain less than 3% of the clay fraction in the weight of the matrix (sand + silt + clay) and are referred to as non-cohesive debris flows. When the clay content is >3%, they are known as cohesive debris flows, which are distinguished by the fact that they do not change their character throughout their runout as non-cohesive types do (Scott and Vallance 1995). The higher clay content in cohesive debris flows is in most cases due to hydrothermal alteration within the volcanic landform, and therefore the resulting clay-rich debris flows originate from volcanic collapses, in contrast with non-cohesive flows, which originate as meltwater surges during eruptions or during excessive precipitation.

5 Causes of Volcanic Collapse in Volcanic Terrains

Volcanic terrains are inherently susceptible to instabilities by nature of their basic materials and structures. Structural failure and collapse is a common outcome of this slope instability. As with nonvolcanic landslides, collapse of volcanic

Fig. 19 Outcrop of slide block within the Big Mountain slide showing fractured and sheared nature of the rock units and preservation of original stratigraphy. Outcrop approximately 6 m high

landforms is produced by a combination of circumstances rather than any single process or cause. For conventional landslides, causes of slope instability have been divided into factors that produce an increase in shear stress (or driving forces) on the slope and into factors that contribute to the reduction in material shear strength and/or friction (e.g., Varnes 1978; Voight and Elsworth 1992). Slope angle is clearly an important factor for increasing shear stress that causes slope instability, especially on stratovolcanoes, as indicated by the frequency of their major slope failures. Precipitation and seismic loading are important destabilizing causes of reducing a material's shear strength on a slope by increasing pore pressures. In many situations, it is the combination of both stress-increasing and strength-deceasing factors that lead to major volcanic landform instabilities.

Once a segment of a volcanic landform has become destabilized, it becomes susceptible to failure in response to one or more internal or external "triggers" that may initiate collapse. This trigger process may operate in the short term (collapse during or immediately after a volcanic event) or with delayed reaction (collapse many years following an event). A comprehensive review of the possible causes and triggers of volcanic landslides can be found in Voight and Elsworth (1997) and del Potro et al. (2013).

5.1 Role of Magma in Volcanic Destabilization

Causes of slope instabilities are inherently due to the nature of the slope, rock composition, layering in relation to strength and permeability zones,

bedding planes, joints, faults, etc. and their orientation relative to the slope (del Potro et al. 2013). Intrusions have a significant role as a primary cause of large volcanic landslides by contributing to these slope instabilities. Intrusions cause intense deformation and visible bulging in all three styles of collapses, as well as producing seismicity and elevated pore-fluid pressure. The internal structure of a volcanic landforms can exhibit intense fracture and faulting caused by intrusions that enhance instability. Hydrothermal alteration affects large segments of volcanic landforms, producing clay minerals that increase permeability and elevate pore-fluid pressures. Such effects can drastically lower shear strength of the rocks, thus weakening the edifice (Lopez and Williams 1993; Frank 1995; Day 1996). Fluid pressure can also be enhanced by hydrothermal waters accompanying large intrusions and dikes (Voight et al. 1983; Elsworth and Voight 1996). Volcanic eruptions continuously add material that lead to oversteepening and overloading at the surface.

The behavior of the subvolcanic substrate is also important, in both subsidence and uplift of the volcanic landforms, to produce slope instabilities. Also, the growth of volcanoes or a volcanic field onto a sloping or weak substrate (e.g., rich in clay or gypsum) enhances the development of lateral spreading and produces instability within and below the volcanic landforms (McGuire 1996).

5.2 Triggers

Destabilization of volcanic landforms may occur over a period of weeks or months, as was the case for the rapid-onset instability produced by the cryptodome intrusion at Mount St. Helens, or destabilization may develop over thousands to tens of thousands of years (McGuire 1996; van Wyk de Vries and Francis 1997). However, once a part of a volcanic terrain has become unstable by one or more causes, it becomes susceptible to failure due to one or more of many triggers that initiate collapse and generate a volcanic landslide. The introduction of new magma within dikes, sills, and laccoliths can trigger structural failure due to increasing pore pressure and reducing shear strength or to over-steepening of surface slopes (Elsworth and Voight 1996). The large amounts of internal and surface deformation produced by intrusions both increases shear stress on the slope and reduces rock shear strength through the creation of shear zones and pervasive brecciation. Changes in the hydrothermal groundwater system increases pore pressure and causes fluid migration. Because the hydrothermal system is driven by intrusions, new intrusions may be responsible for disturbances in the system and thus trigger a landslide (van Wyk de Vries and Davies 2015). Additional extrusive material added onto already heavily loaded volcanic landforms may also initiate failure and collapse. Other triggers involve earthquakes (typically > M5) that may quickly change pore pressure (Acocella et al. 2003), and displacements associated with long-term structural spreading (van Wyk de Vries and Francis 1997). Environmental factors may also be important triggers, such as large precipitation events or higher sea levels at island volcanoes, both of which may elevate pore pressures.

6 Volcanic Landslide Transport and Mobility Mechanisms

Once failure has been initiated, the failed mass moves with considerable inertial energy and may travel in a largely coherent manner, or the mass may be totally disaggregated with travel velocities of over 100 m/s during catastrophic failure. Velocities of volcanic debris avalanches have been calculated in the order of 50–150 m/s (Ui et al. 1986; Siebert et al. 1995), whereas direct measurements of the only observed avalanche (from Mount St. Helens), provides an average velocity of 35 m/s and initial velocities ranging from 70 to 80 m/s (Voight et al. 1981).

One of the first approaches used to determine debris avalanche mobility was based on the apparent coefficient of friction (H/L), using the relationship between the drop height and the maximum runout length of the flow (Hsü 1975). This parameter has been largely used to describe flow mobility, which generally increases as the mass (volume) increases (Dade and Huppert 1998). Therefore, larger volumes generally mean longer runouts as well as higher velocities. Some large avalanches have been known to carry blocks as long as three kilometers several kilometers from their source (Francis 1993).

Despite our observations on volcanic landslides, understanding the physical processes operating during exceptionally long run-out distances is still problematic. Several dynamic models about flow behavior and mechanism of emplacement have been proposed, ranging from fluidized granular flow (Bagnold 1954; Melosh 1983; Davies 1982; Campbell 1990) to plug flow (Takarada et al. 1999). Movement occurs over a lubricated, shearing basal layer that allows much of the mobility yet has minimal frictional effects (Voight et al. 1983; Reubi and Hernandez 2000; Clavero et al. 2002; Shea et al. 2008). A large list of transport mechanisms has been proposed to explain reduced friction of large avalanches, including fine basal powders, interstitial fluids, pore-fluid pressure, an air cushion, dispersive grain flow, local steam generation, frictional melting, lubrication, fluidization, entrainment, oscillation, and dynamic fragmentation (Kent 1966; Shreve 1968; Howard 1973; Hsü 1975; Lucchitta 1978; McSaveney 1978; Davies 1982; McEwen 1989; Iverson 1997; Davies and McSaveney 1999; van Wyk de Vries et al. 2001; Legros 2002; Collins and Melosh 2003; Aharonov and Anders 2006; Campbell 2006; Mangeney et al. 2007; Pudasaini and Hutter 2007; Deganutti 2008; Cagnoli and Quareni 2009; McSaveney and Davies 2009; Davies et al. 2010). Of these different mechanisms, no one dominant mechanism stands out as an explanation for the hypermobility of huge slides and avalanches (Pudasaini and Miller 2013).

7 Hazards

The hazards that volcanic landslides at volcanoes, laccoliths, and volcanic fields can produce are numerous. Landslides can travel large distances and destroy everything in their paths, and they can dam rivers and lakes to produce flooding. It has been shown that landslides can lead to a decrease in magma pressure and cause an explosive volcanic eruption. The mixture of water with debris from an avalanche may produce debris flows that have much greater mobility, so can affect people living in valley areas far away from the source of the avalanche.

Hazards of volcanic landslides can be amplified by eruptions that are triggered by, or accompany, collapse of their unstable slopes. These associated eruptions can range from mild to moderate phreatic explosions to major Plinian eruptions, along with powerful lateral blasts from sudden depressurization of hydrothermal-magmatic systems.

Debris avalanches may convert to debris flows that travel considerably farther than avalanches and cover broad valley areas with great impact. Debris flows can form directly by transformation from debris avalanches during displacement, from dewatering of debris avalanche deposits shortly after emplacement, or from breakouts of avalanche-dammed lakes weeks to years after the avalanche (Pierson 1985; Fairchild 1987; Scott et al. 1995; Vallance and Scott 1997; Siebert 2002).

Another important hazard that can be produced from volcanic landslides are tsunamis. Historically, the most deadly volcanic landslide occurred in 1792 when sliding debris from Mt. Mayu-yama near Unzen Volcano in Japan plummeted into the Ariaka Sea and generated a tsunami that reached the opposite shore 20 km away, killing nearly 15,000 people in the process (Siebert 2002). The effect of tsunamis generated by volcanic landslides entering the seas or lakes is considerable. Nearly 80% of the ~25,000 historical fatalities from volcanic landslides came from those that generated tsunamis upon entering the water.

8 Summary

Most studies of volcanic structural failure and collapse have concentrated on volcano flanks, yet other volcanic landforms in volcanic terrains have produced collapse features that rival or surpass them in scale. These include slope failures from laccoliths and volcanic fields, both of which produced volcanic landslides that share many morphological and textural similarities with volcanic landslides from volcanoes. Subvolcanic magma systems may play an integral part in the collapse of all three volcanic collapse types by creating elevated landforms with steep slopes, by aiding in destabilizing slopes, and locally by triggering a slope failure. Some slope failures even triggered volcanic eruptions similar to, but larger than, those produced at Mount St. Helens. Although large-scale catastrophic collapse of volcanic fields are rare, they represent the largest know subaerial volcanic landslides on Earth.

Acknowledgements We gratefully acknowledge support from the Utah Geological Survey, the U.S. Geological Survey (National Cooperative Geologic Mapping Program) through a number of USGS STATEMAP grants, and the Kent State University Research Council. We also are grateful for generous cooperation and logistical support from the U.S. Forest Service and U.S. Geological Survey through the BARCO (Basin and Range-Colorado Plateau transition area) project. We would also like to thank Lee Siebert and Christoph Breitkreuz for helpful reviews of this manuscript.

References

Acocella V (2005) Modes of sector collapse of volcanic cones: Insights from analogue experiments. J Geophys Res. Solid Earth 110(B2)

Acocella V, Behncke B, Neri M, D'Amico S (2003) Link between large-scale flank slip and 2002–2003 eruption at Mt. Etna (Italy). Geophys Res Lett 30(24):2286

Aharonov E, Anders MH (2006) Hot water: a solution to the Heart Mountain detachment problem? Geology 34 (3):165–168

Arguden AT, Rodolfo KS (1990) Sedimentologic and dynamic differences between hot and cold laharic debris flows of Mayon Volcano, Philippines. Geol Soc Am Bull 102(7):865–876

Bagnold RA (1954) Experiments on a gravity-free dispersion of large solid spheres in a Newtonian fluid under shear. Proc R Soc Lond Ser A 225:49–63

Belousov AB (1995) The Shiveluch volcanic eruption of 12 November 1964—explosive eruption provoked by failure of the edifice. J Volcanol Geotherm Res 66:357–365

Belousov AB (1996) Deposits of the 30 March 1956 directed blast at Bezymianny volcano, Kamchatka, Russia. Bull Volcanol 57:649–662

Beutner EC, Hauge TA (2009) Heart Mountain and South Fork fault systems—architecture and evolution of the col-lapse of an Eocene volcanic system, northwest Wyoming. Rocky Mt Geol 44(2):147–164

Biek RF, Rowley PD, Hayden JM, Hacker DB, Willis GC, Hintze LF, Anderson RE, Brown KD (2009) Geologic Map of the St. George and East Part of the Clover Mountains 30' × 60' quadrangles, Washington and Iron Counties, Utah. Utah Geological Survey Map 242, scale 1:100,000

Biek RF, Hacker DB, Rowley PD (2014) New constraints on the extent, age, and emplacement history of the early Miocene Markagunt Megabreccia, southwest Utah—the deposit of one of the world's largest subaerial gravity slides. In: MacLean JS, Biek RF, Huntoon JF (eds) Geology of Utah's far south, vol 43. Utah Geological Association Publication, pp 565–598

Biek RF, Rowley PD, Anderson JJ, Maldonado F, Moore DW, Hacker DB, Eaton JG, Hereford R, Sable EG, Filkorn HF, Matyjasik B (2015) Geologic map of the Panguitch 30' × 60' quadrangle, Garfield, Iron, and Kane Counties, Utah. Utah Geological Survey Map 270DM, scale 1:62,500

Blank HR, Rowley PD, Hacker DB (1992) Miocene monzonitic intrusions and associated megabreccias of the Iron Axis region, southwestern Utah. In: Wilson JR (ed) Field guide to geologic excursions in Utah and adjacent areas of Nevada, Idaho, and Wyoming. Utah Geological Survey Miscellaneous Publication 92-3, pp 399–420

Blank Jr HR, Mackin JH (1967) Geologic interpretation of an aeromagnetic survey of the Iron Springs district, Utah. U.S. Geological Survey Professional Paper, 516-B

Bulmer, MH, Guest, JE (1996) Modified volcanic domes and associated debris aprons on Venus. In: McGuire WJ, Jones AP, Neuberg J (eds) Volcano instability on the Earth and Other planets. Geological Society Special Publication

Cagnoli B, Quareni F (2009) Oscillation-induced mobility of flows of rock fragments with quasi-rigid plugs in rectangular channels with frictional walls: a hypothesis. Eng Geol 103(1–2):23–32

Campbell CS (1990) Rapid granular flows. Annu Rev Fluid Mech 22(1):57–90

Campbell CS (2006) Granular material flows—an overview. Powder Technol 162:208–229
Carracedo JC (1994) The Canary Islands: an example of structural control on the growth of large oceanic-island volcanoes. J Volcanol Geotherm Res 60:225–241
Carrasco-Núñez G, Siebert L, Capra L (2011) Hazards from volcanic avalanches. Horizons in earth science research. Nova Science Publishers, New York
Clavero JE, Sparks RSJ, Huppert HE (2002) Geological constraints on the emplacement mechanism of the Parinacota debris avalanche, northern Chile. Bull Volcanol 64:40–54
Collins GS, Melosh HJ (2003) Acoustic fluidization and the extraordinary mobility of sturzstroms. J Geophys Res 108(B10):2473
Costa JE (1988) Floods from dam failures. In: Baker VR, Kochel RC, Patton PC (eds) Flood geomorphology. Wiley, New York, pp 439–463
Costa JE, Shuster RL (1988) The formation and failure of natural dams. Geol Soc Am Bull 100:1054–1068
Craddock JP, Malone DH, Magloughlin J, Cook AL, Rie-ser ME, Doyle JR (2009) Dynamics of the emplacement of the Heart Mountain allochthon at White Mountain—constraints from calcite twinning strains, anisotropy of magnetic susceptibility, and thermodynamic calculations. Geol Soc Am Bull 121 (5/6):919–938
Crandell DR (1989) Gigantic debris-avalanche of Pleistocene age from ancestral Mount Shasta volcano, California, and debris avalanche hazard zonation. Bulletin of the US Geological Survey, 1861
Crandell DR, Miller CD, Glicken HX, Christiansen RL, Newhall CG (1984) Catastrophic debris avalanche from ancestral Mount Shasta volcano, California. Geology 12:143–146
Cruden DM, Varnes DJ (1996) Landslide types and processes. In: Turner AK, Schuster RL (eds) Landslides investigation and mitigation. Transportation Research Board, U.S. National Research Council, Special Report 247, chap. 3, pp 36–75
Crumpler LS, Head JW, Aubele JC (1996) Calderas on Mars: characteristics, structure, and associated flank deformation. In: McGuire WJ, Jones AP, Neuberg J (eds) Volcano instability on the Earth and other planets. Geological Society Special Publication
Dade WB, Huppert HE (1998) Long-runout rockfalls. Geology 26(9):803–806
Davies TRH (1982) Spreading of rock avalanche debris by mechanical fluidization. Rock Mech 15:9–24
Davies TR, McSaveney MJ (1999) Runout of dry granular avalanches. Can Geotech J 36(2):313–320
Davies T, McSaveney M, Kelfoun K (2010) Runout of the Socompa volcanic debris avalanche, Chile: a mechanical explanation for low basal shear resistance. Bull Volc 72(8):933–944
Day S (1996) Hydrothermal pore fluid pressure and the stability of porous, permeable volcanoes. In: McGuire WJ, Jones AP, Neuberg J (eds) Volcano instability on the Earth and other Planets. Geological Society London Special Publication, vol 110, pp 77–94
Deganutti AM (2008) The hypermobility of rock avalanches. (PhD Dissertation, Universita delgi Studi di Padova)
del Potro R, Hürlimann M, Pinkerton H (2013) Modelling flank instabilities on stratovolcanoes: parameter sensitivity and stability analyses of Teide, Tenerife. J Volcanol Geotherm Res 256:50–60
Elsworth D, Voight B (1996) Evaluation of volcano flank instability triggered by dyke intrusion. Spec Pub Geol Soc Lond 110:45–54
Fairchild LH (1987) The importance of lahar initiation processes. Rev Eng Geol 7:51–61
Frank D (1995) Surficial extent and conceptual model of hydrothermal system at Mount Rainier, Washington. J Volcanol Geotherm Res 65:51–80
Francis P (1993) Volcanoes, a planetary perspective. Oxford University Press, Oxford, p 443
Francis PW, Gardeweg M, Ramirez CF, Rothery DA (1985) Catastrophic debris avalanche deposit of Socompa volcano, northern Chile. Geology 13:600–603
Glicken H (1986) Rockslide—debris avalanche of May 18, 1980, Mount St. Helens volcano. PhD dissertation, Univ Santa Barbara, 303 p
Glicken H (1991) Rockslide-debris avalanche of May 18th, 1980, Mount St. Helens volcano. US Geological Survey Professional Paper, Washington, p 1488
Glicken H (1996) Rockslide-debris avalanche of May 18, 1980, Mount St. Helens Volcano, Washington. U.S. Geological Survey Open-File Report 96-677, 90 p
Glicken H (1998) Rockslide-debris avalanche of May 18, 1980, Mount St. Helens Volcano, Washington. Bull Geol Surv Japan 49(2/3):55–106
Gorshkov GS (1959) Gigantic eruption of the volcano Bezymianny. Bull Volcanol 20:77–109
Gorshkov GS, Dubik YM (1970) Gigantic directed blast at Shiveluch volcano (Kamchatka). Bull Volcanol 34:261–288
Hacker DB, (1998) Catastrophic gravity sliding and volcanism associated with the growth of laccoliths—examples from early Miocene hypabyssal intrusions of the Iron Axis magmatic province, Pine Valley Mountains, southwestern Utah. Kent, Ohio, Kent State University, Ph.D. dissertation, 258 p
Hacker DB, Rowley PD, Blank HR, Snee LW (1996) Early Miocene catastrophic gravity sliding and volcanism associated with intrusions of the southern Iron Axis region, southwest Utah. Geol Soc Am Abstr Programs 29:511
Hacker DB, Holm DK, Rowley PD, Blank HR (2002) Associated Miocene laccoliths, gravity slides, and volcanic rocks, Pine Valley Mountains and Iron Axis region, south-western Utah. In: Lund WR (ed) Field guide to geo-logic excursions in southwestern Utah and adjacent areas of Arizona and Nevada. U.S.

Geological Survey Open-File Report OF 02-0172, pp 235–283
Hacker DB, Petronis MS, Holm DK, and Geissman JW (2007) Shallow level emplacement mechanisms of the Mi-ocene Iron Axis laccolith group, southwest Utah. In: Lund WR (ed) Field guide to geologic excursions in southern Utah. Utah Geological Association Publication vol 35, p 49
Hacker DB, Biek RF, Rowley PD (2014) Catastrophic emplacement of the gigantic Markagunt gravity slide, southwest Utah (USA). Implications for hazards associated with sector collapse of volcanic fields. Geology 42(11):943–946
Herrick JA, Siebert L, Rose WI (2013) Large-volume Barriles and Caisán debris avalanche deposits from Volcán Barú, Panama. Geol Soc Am Spec Pap 498:141–162
Hoblitt RP, Miller CD, Vallance JW (1981) Origin and stratigraphy of the deposit produced by the May 18 directed blast. In: Lipman PW, Mullineaux DR (eds) The 1980 eruptions of Mount St. Helens, Washington, vol 1250. U.S. Geol Surv Prof Paper, pp 401–419
Howard KA (1973) Avalanche mode of motion: implications from lunar examples. Science 180:1052–1055
Hsü KJ (1975) Catastrophic debris stream (Sturzstroms) generated by rockfalls. Geol Soc Amer Bull 86:129–140
Hsü KJ (1978) Albert Heim: observations on landslides and relevance to modern interpretations. Rockslides Avalanches. 1:71–93
Iverson RM (1997) The physics of debris flows. Rev Geophys 35:245–296
Keating BH, McGuire WJ (2000) Island edifice failures and associated tsunami hazards. Pure appl Geophys 157(6-8):899–955
Kent PE (1966) The transport mechanism in catastrophic rock falls. J Geol 74:79–83
Komorowski JC, Boudon G, Semet M, Beauducel F, Anténor-Habazac C, Bazin S, Hammouya G (2005) Guadeloupe. In: Lindsay J, Robertson R, Shepherd J, Ali S (eds) Volcanic hazard atlas of the Lesser Antilles. University of the West Indies, Seismic Research Unit, Trinidad and IAVCEI, pp 65–102
Komorowski JC, Glicken HX, Sheridan MF (1991) Secondary electron imagery of microcracks and hackly fracture surfaces in sand-size clasts from the 1980 Mount St. Helens debris-avalanche deposit: implications for particle-particle interactions. Geology 19(3):261–264
Kuntz MA, Rowley PD, MacLeod NS (1990) Geologic maps of pyroclastic-flow and related deposits of the 1980 eruptions of Mount St. Helens, Washington. U. S. Geological Survey Miscellaneous Investigations Series Map I-1950, scale 1:12,000
Legros F (2002) The mobility of long runout landslides. Eng Geol 63:301–331
Lipman PW, Mullineaux D (eds) (1981) The 1980 eruptions of Mount St. Helens. US Geological Survey Professional Paper, 1250
Lipman PW, Rhodes JM, Dalrymple GB (1991) The Ninole Basalt—implications for the structural evolution of Mauna Loa volcano, Hawaii. Bull Volcanol 53:1–19
Lopez DL, Williams SN (1993) Catastrophic volcanic collapse: relation to hydrothermal processes. Science 260:1794–1796
Lucchitta BK (1978) A large landslide on Mars. Geol Soc Am Bull 89:1601–1609
Mackin JH (1960) Structural significance of Tertiary volcanic rocks in southwestern Utah. Am J Sci 258 (2):81–131
Malone DH, Craddock JP (2008) Recent contributions to the understanding of the Heart Mountain detachment, Wyoming. Northwest Geol 37:21–40
Mangeney A, Tsimring LS, Volfson D, Aranson IS, Bouchut F (2007) Avalanche mobility induced by the presence of an erodible bed and associated entrainment. Geophys Res Lett 34:L22401
McEwen AS (1989) Mobility of large rock avalanches: evidence from Valles Marineris, Mars. Geology 17:1111–1114
McGuire WJ (1996) Volcano instability: a review of contemporary themes. In: McGuire WJ, Jones AP, Neuberg J (eds) Volcano instability on the earth and other planets. Geological Society Special Publication
McGuire WJ (2006) Lateral collapse and tsunamigenic potential of marine volcanoes. Geol Soci London Spec Publ 269(1):121–140
McSaveney MJ (1978) Sherman glacier rock avalanche, Alaska, U.S.A. In: Voight B (ed) Natural phenomena. Rockslides and avalanches, vol 1. Elsevier Sci., New York, pp 197–258
McSaveney MJ, Davies TRH (2009) Surface energy is not one of the energy losses in rock comminution. Eng Geol 109:109–113
Mehl KW, Schmincke HU (1999) Structure and emplacement of the Pliocene Roque Nublo debris avalanche deposit, Gran Canaria, Spain. J Volcanol Geoth Res 94(1):105–134
Melosh HJ (1983) Acoustic fluidization: can sound waves explain why dry rock debris appears to flow like a fluid in some energetic geologic events? Am Sci 71:158–165
Moore JG, Clague DA, Holcomb RT, Lipman PW, Normark WR, Torresan ME (1989) Prodigious submarine landslides on the Hawaiian Ridge. J Geophys Res 94:17465–17484
Moore JG, Normark WR, Holcomb RT (1994) Giant Hawaiian landslides. Ann Rev Earth Planet Sci 22:119–144
Palmer BA, Neall VE (1989) The Murimotu Formation-9500 year old deposits of a debris avalanche and associated lahars, Mount Ruapehu, North Island, New Zealand. J Geol Geophys 32:477–486
Petronis MS, Hacker DB, Holm DK, Geissman JW, Harlan SS (2004) Magmatic flow paths and paleomagnetism of the Miocene Stoddard Mountain Laccolith, Iron Axis region, southwest Utah, USA.

In: Martin-Hernandez F, Luneburg CM, Aubourg C, Jackson M (eds) Magnetic fabric: methods and applications, vol 238. The Geological Society of London, Special Publications, pp 251–283

Pierson TC (1985) Initiation and behavior of the 1980 Pine Creek and Muddy River lahars, Mount St. Helens, Washington. Geol Soc Am Bull 96:1056–1069

Pierson TC, Costa JE (1987) A rheologic classification of subaerial sediment-water flows. In: Costa JE, Wieczorek GF (eds) Debris flows/Avalanches: process, recognition, and mitigation. Geol. Soc. Am. Rev. Eng. Geol., pp 1–12

Ponomareva VV, Melekestsev IV, Dirksen OV (2006) Sector collapses and large landslides on late Pleistocene-Holocene volcanoes in Kamchatka, Russia. J Volc Geotherm Res 158:117–138

Pulgarin B, Macas JL, Cepeda H (1999) Secondary debris flow originated from the dam failure of a Pleistocene debris avalanche deposit, Nevado del Huila Volcanic Complex, Colombia. Am. Geophys. Union Fall Meeting. Eos, Trans. Am. Geophys. Union, San Francisco, CA, p. V31D-02

Pudasaini SP, Hutter K (2007) Avalanche dynamics: dynamics of rapid flows of dense granular avalanches. Springer, Berlin, New York

Pudasaini SP, Miller SA (2013) The hypermobility of huge landslides and avalanches. Eng Geol 157:124–132

Reubi O, Hernandez J (2000) Volcanic debris avalanche deposits of the upper Maronne valley (Cantal volcano, France): evidence for contrasted fromation and transport mechanism. J Volcanol Geotherm Res 102:271–286

Rowley PD (1998) Cenozoic transverse zones and igneous belts in the Great Basin, western United States: their tectonic and economic implications. Special Papers-Geological Society of America, pp 195–228

Rowley PD, Cunningham CG, Steven TA, Mehnert HH, Naeser CW (1998) Cenozoic igneous and tectonic setting of the Marysvale volcanic field and its relation to other igneous centers in Utah and Nevada. In: Laccolithic complexes of southeastern Utah: time of emplacement and tectonic setting—workshop proceedings, pp 167–201

Rowley PD, Cunningham CG, Steven TA, Workman JB, Anderson JJ, Theissen KM (2002) Geologic map of the central Marysvale volcanic field, southwestern Utah. U.S. Geological Survey Geologic Investigations Series Map I-2645-A, scale 1:100,000

Rowley PD, Kuntz MA, MacLeod NS (1981) Pyroclastic-flow deposits. In: Lipman PW, Mullineaux DR (eds) The 1980 eruptions of Mount St. Helens, Washington. U.S. Geological Survey Professional Paper, vol 1250, pp 489–512

Rowley PD, MacLeod NS, Kuntz MA, Kaplan AM (1985) Proximal bedded deposits related to pyroclastic flows of May 18, 1980, Mount St. Helens, Washington. Geol Soc Am Bull 96:1373–1383

Rowley PD, Vice GS, McDonald RE, Anderson JJ, Machette MN, Maxwell DJ, Ekren EB, Cunningham CG, Steven TA, Wardlaw BR (2005) Interim geologic map of the Beaver 30' × 60' quadrangle, Beaver, Piute, Iron, and Garfield Counties, Utah. Utah Geological Survey Open-File Report 454, scale 1:100,000

Rowley PD, Williams VS, Vice GS, Maxwell DJ, Hacker DB, Snee LW, Mackin JH (2006) Interim geologic map of the Cedar City 30' × 60' quadrangle, Iron and Washington Counties, Utah. Utah Geological Survey Open-File Report 476DM, scale 1:100,000

Schuster RL, Crandell, DR, (1984) Catastrophic debris avalanches from volcanoes. In: IV international symposium on landslide proceedings, Toronto, vol 1, pp 567–572

Scott KM, Vallance JW (1995) Debris flow, debris avalanche, and flood hazards at and downstream from Mount Rainier, Washington. U.S. Geological Survey Hydrologic Investigations Atlas 729: 2 Sheets and Accompanying Pamphlet

Scott KM, Vallance JW, Pringle PT (1995) Sedimentology, behavior and hazards of debris flows at Mount Rainier, Washington. U.S. Geological Survey Professional Paper 1547, 56 p

Scott KM, Macias JL, Vallance JW, Naranjo JA, Rodriguez-Elizarraras SR, McGeehin JP (2002) Catastrophic debris flows transformed from landslides in volcanic terrains: mobility, hazard assessment, and mitigation strategies. US Geological Survey Professional Paper, 1630

Scott KM, Vallance JW, Kerle N, Luis Macías J, Strauch W, Devoli G (2005) Catastrophic precipitation-triggered lahar at Casita volcano, Nicaragua: occurrence, bulking and transformation. Earth Surf Proc Land 30(1):59–79

Shea T, van Wyk de Vries B, Pilato M (2008) Emplacement mechanisms of contrasting debris avalanches at Volcan Mombacho (Nicaragua), provided by structural and facies analysis. Bull Volcanol 70:899–921

Shreve RL (1968) The Blackhawk landslide. Geol Soc Am Spec Pap 108:47

Siebert L (1984) Large volcanic debris avalanches: characteristics of source areas, deposits, and associated eruptions. J Volcanol Geotherm Res 22:163–197

Siebert L (1992) Threats from debris avalanches. Nature 356:658–659

Siebert L (1996) Hazards of large volcanic debris avalanches and associated eruptive phenomena. In: Scarpa T, Tilling RI (eds) Monitoring and mitigation of volcanic hazards. Springer, Berlin, pp 541–572

Siebert L (2002) Landslides resulting from structural failure of volcanoes. In: Evans SG, De Graff JV (eds) Catastrophic landslides: effects, occurrence, and mechanisms, vol 15. Geol Soc Amer Rev Eng Geol, pp 209–235

Siebert L, Glicken H, Ui T (1987) Volcanic hazards from Bezymianny- and Bandai-type eruptions. Bull Volcanol 49:435–459

Siebert L, Béget JE, Glicken H (1995) The 1883 and late-prehistoric eruptions of Augustine volcano, Alaska. J Volcanol Geotherm Res 66:367–395

Siebert L, Alvarado GE, Vallance JW, van Wyk de Vries B (2006) Large-volume volcanic edifice failures in Central America and associated hazards. In: Rose WI, Bluth GJS, Carr MJ, Ewert JW, Patino LC, Vallance JW (eds) Volcanic hazards in Central America, Geological Society of America Special Paper, vol 412, pp 1–26

Siebert L, Simkin T, Kimberly P (2010) Volcanoes of the World, 3rd edn. University of California Press, Berkeley, p 551

Stoopes GR, Sheridan MF (1992) Giant debris avalanches from the Colima Volcanic Complex, Mexico: implications for long runout landslides (>100 km) and hazard assessment. Geology 20:299–302

Takarada T, Ui T, Yamamoto H (1999) Depositional features and transportation mechanism of valley filling Iwasegawa and Kaida debris avalanches, Japan. Bull Volcanol 60:508–522

Ui T (1983) Volcanic debris avalanche deposits—identification and comparison with non-volcanic debris stream deposits. J Volcanol Geotherm Res 18:135–150

Ui T, Yamamoto H, Suzuki-Kamata K (1986) Characterization of debris avalanche deposits in Japan. J. Volcanol Geotherm Res 29:231–243

Ui T, Takarada S, Yoshimoto M (2000) Debris avalanches. Encycl Volcanoes 617–626

Vallance JW, Scott KM (1997) The Osceola Mudflow from Mount Rainier: sedimentology and hazard implications of a huge clay-rich debris flow. Geol Soc Am Bull 109:143–163

van Wyk de Vries B, Francis P (1997) Catastrophic collapse at stratovolcanoes induced by gradual volcano spreading. Nature 387:387–390

van Wyk de Vries B, Self S, Francis, PW Keszthelyi L (2001) A gravitational spreading origin for the Socompa debris avalanche. J Volcanol Geotherm Res 105:225–247

van Wyk de Vries B, Davies T (2015) Landslides, debris avalanches and volcanic gravitational deformation. In: Sigurdsson H, Houghton B, McNutt S, Rymer H, Stix J (eds) The encyclopedia of volcanoes, 2nd edn, pp 665–685

van Wyk de Vries B, Delcamp A (2015) Chapter 5—volcanic debris avalanches. In: Landslide hazards, risks and disasters. Academia Press

Varnes DJ (1978) Slope movement types and processes, In: Schuster RL, Krizek RJ (eds) Landslides, analysis and control. National Research Council, Transportation Research Board, Special Report, vol 176, pp 11–33

Voight B (ed) (1978) Rockslides and avalanches 1, natural phenomena. Elsevier, Amsterdam, 826 p

Voight B (1981) Time scale for the first movements of the May 18 eruption. In: Lipman PW, Mullineaux DR (eds) The 1980 eruptions of Mount St. Helens, Washington. US Geological Survey Professional Paper, vol 1250, pp 69–86

Voight B, Elsworth D (1992) Resolution of mechanics problems for prodigious Hawaiian landslides: magmatic intrusions simultaneously increase driving force and reduce driving resistance by fluid pressure enhancement (abstract). Eos Trans. AGU 73 43, 506, Fall Meeting suppl

Voight B, Elsworth D (1997) Failure of volcano slopes. Geotechnique 47(1):1–31

Voight B, Glicken H, Janda RJ, Douglass PM (1981) Catastrophic rockslide avalanche of May 18. In: Lipman PW, Mullineaux DR (eds) The 1980 eruptions of Mount St. Helens, Washington. US Geological Survey Professional Paper, vol 1250, pp 347–348

Voight B, Janda RJ, Glicken H, Douglass PM (1983) Nature and mechanics of the Mount St. Helens rockslide-avalanche of 18 May 1981. Geotechnique 33:243–273

Voight B, Komorowski J C, Norton G E, Belousov A, Belousova M, Boudon G, Francis PW, Franz W, Heinrich P, Sparks RSJ, Young SR (2002) The 26 December (Boxing Day) 1997 sector collapse and debris avalanche at Soufrière Hills Volcano, Montessat. In: Druitt TH, Kokelaar P (eds) The eruption of Soufrière Hills Volcano, Montserrat, from 1995 to 1999. The Geoll Soc London, Mem, vol 21, pp 363–407

Wadge G, Francis PW, Ramirez CF (1995) The Socompa collapse and avalanche event. J Volcanol Geotherm Res 66:309–336

Yokoyama I (2002) Growth mechanism of the 1944 lava dome of Usu volcano in Hokkaido, Japan. Proc Japan Acad, Ser B 78(1):6–11